Applied Catalysis B: Environmental 88 (2009) 1–24

Contents lists available at ScienceDirect

Applied Catalysis B: Environmental

journal homepage: www.elsevier.com/locate/apcatb

Review

Carbon supports for low-temperature fuel cell catalysts

Ermete Antolini

Scuola di Scienza dei Materiali, Via 25 aprile 22, 16016 Cogoleto (Genova), Italy

ARTICLE INFO

Article history:
Received 18 July 2008
Received in revised form 24 September 2008
Accepted 26 September 2008
Available online 9 October 2008

Keywords:
Fuel cells
Catalysts
Platinum
Carbon
Nanomaterials

ABSTRACT

To increase their electrochemically active surface area, catalysts supported on high surface area materials, commonly carbons, are widely used in low-temperature fuel cells. Recent studies have revealed that the physical properties of the carbon support can greatly affect the electrochemical properties of the fuel cell catalyst. It has been reported that carbon materials with both high surface area and good crystallinity can not only provide a high dispersion of Pt nanoparticles, but also facilitate electron transfer, resulting in better device performance. On this basis, novel non-conventional carbon materials have attracted much interest as electrocatalyst support because of their good electrical and mechanical properties and their versatility in pore size and pore distribution tailoring. These materials present a different morphology than carbon blacks both at the nanoscopic level in terms of their pore texture (for example mesopore carbon) and at the macroscopic level in terms of their form (for example microsphere). The examples are supports produced from ordered mesoporous carbons, carbon aerogels, carbon nanotubes, carbon nanohorns, carbon nanocoils and carbon nanofibers. The challenge is to develop carbon supports with high surface area, good electrical conductivity, suitable porosity to allow good reactant flux, and high stability in fuel cell environment, utilizing synthesis methods simple and not too expensive.

This paper presents an overview of carbon supports for Pt-based catalysts, with particular attention on new carbon materials. The effect of substrate characteristics on catalyst properties, as electrocatalytic activity and stability in fuel cell environment, is discussed.

Contents

E-mail address: ermantol@libero.it.

0926-3373/$ – see front matter © 2008 Elsevier B.V. All rights reserved.
doi:10.1016/j.apcatb.2008.09.030

1. Introduction

Low-temperature fuel cells, with either hydrogen (phosphoric acid fuel cell, PAFC, and polymer electrolyte membrane fuel cell, PEMFC), methanol (direct methanol fuel cell, DMFC) or ethanol (direct ethanol fuel cell, DEFC) as the fuel, represent an environmentally friendly technology and are attracting considerable interest as a means of producing electricity by direct electrochemical conversion of hydrogen/methanol/ethanol and oxygen into water/water and carbon dioxide [1,2]. Platinum and platinum alloys are used as anode and cathode catalysts in low-temperature fuel cells. Since the activity of a catalyst increases as the reaction surface area of the catalyst increases, catalyst particles should be reduced in the diameter to increase the active surface. It has to take into account, however, that the specific activity of the metal nanoparticles can decrease with decreasing the particle size (particle-size effect) [3–6]. So the catalysts are supported on a high surface area substrate. The structure and proper dispersal of these metal particles make low loading catalyst feasible for fuel cell operation. In addition to a high surface area, which may be obtained through high porosity, a support for a fuel cell catalyst must also have sufficient electrical conductivity so that the support can act as a path for the flow of electrons. Moreover, carbon supports should have a high percentage of mesopores in the 20–40 nm region to provide a high accessible surface area to catalyst and to monomeric units of the Nafion ionomer and to boost the diffusion of chemical species. The formation of carbon black (CB) supported platinum and platinum alloy catalysts for low-temperature fuel cells was reviewed by Antolini [7,8]. Aside from the dispersion effect of the support material, an interaction effect between the support material and the metal catalysts exists. Since the catalysts are bonded to the support, the support material can potentially influence the activity of the catalyst. This interaction effect can be explained in two distinct ways. First, the support material can modify the electronic character of the catalyst particles. This electronic effect could affect the reaction characteristics of the active sites present on the catalyst surface. The second is a geometric effect. The support material could also modify the shape of the catalyst particles. That is, those effects could change the activity of catalytic sites on the metal surface and modify the number of active sites present [9]. Moreover, the substrate may bring its own (electro)chemical function, which is the case for RuO_x or WO_x substrates for ORR or methanol/CO oxidation [10–13]. On this basis, an important issue of the research in the field of the fuel cells is addressed on the development of new carbon and non-carbon supports, which could improve the electrochemical activity of the catalysts.

The stability of the catalyst support in fuel cell environment is of great importance in the development of new substrates. In addition to high surface area, porosity and electrical conductivity, corrosion resistance is also an important factor in the choice of a good catalyst support. If the catalyst particles cannot maintain their structure over the lifetime of the fuel cell, change in the morphology of the catalyst layer from the initial state will result in a loss of electrochemical activity. For these catalysts more severe requirements have to be met to achieve the required long-term stability of 40,000–60,000 h. Due to the presence of oxygen, support corrosion may occur. Indeed, during the development of the phosphoric acid fuel cell system it was found that the carbon catalyst support degraded over time and that this was a potential problem for this type of fuel cells. It was found that carbon is lost from the system through oxidation leading to significant losses of carbon over a short period of time. The acid environment in the PEMFCs is different from that of PAFCs. The PEMFCs operate at less than 100 °C, as compared with the PAFCs, which operate at higher temperature (180 °C). Then, a better stability of the substrate in the PEMFC environment is expected. Carbon support stability problems, however, can be present for high-temperature (>100 °C) PEMFCs [14,15].

Up to 1990s carbon blacks were almost exclusively used as catalysts support in low-temperature fuel cells. To improve the electrochemical activity and stability of the catalysts, in the last years new carbon materials have been tested as support for fuel cell catalysts. With respect to carbon blacks, these new carbon materials are different both at the nanoscopic level in terms of their structural conformation (for example nanotubes) and pore texture (for example mesopore carbons) and/or at the macroscopic level in terms of their form (for example microspheres). Auer et al. [16] reviewed the use of activated carbons, carbon blacks and graphites as well as graphitized materials as support materials for metal powder catalysts. Rodriguez-Reinoso [17] dealt with the surface chemistry of carbon supports and the influence of the oxygen groups on the carbon surface upon the properties of the supported catalysts. The purpose of this paper is to provide a better insight into the characteristics and stability of fuel cell catalyst supports, in the light of the latest advances on this field.

2. Carbon blacks and graphite materials

Carbon blacks are widely used as catalyst support in low-temperature fuel cells. They are manufactured by the pyrolysis of hydrocarbons such as natural gas or oil fractions from petroleum processing [18]. Due to the nature of the starting materials, the ash content of carbon black is very low, frequently well below 1 wt%. The carbon blacks are produce by the oil-furnace processes and acetylene processes. The most important production method is the furnace black process in which the starting material is fed to a furnace and burned with a limited supply of air at about 1400 °C. Due to its low cost and high availability, oil-furnace carbon black (e.g. Vulcan XC-72) has been used widely as the support for platinum catalyst in low-temperature fuel cells. The characteristics of some oil-furnace and acetylene carbon blacks are reported in Table 1 [19,20]. It has to be remarked that Vulcan is not a well-defined oil-furnace black material. Its particles are not mono-dispersed.

High surface area graphite (HSAG) is available from graphitized material by a special grinding process. Surface areas of 100–

Table 1
Catalysts supports of various carbon blacks. AB: acetylene black; FB: oil-furnace black.

Carbon black	Maker	Surface area ($m^2\ g^{-1}$)	Particle size (nm)
Denka black AB [19]	Denkikagaku kogyo	58	40
Exp. sample AB [19]	Denkikagaku kogyo	835	30
Shavinigan AB [20]	Gulf Oil	70–90	40–50
Conductex 975 FB [19]	Columbian	250	24
Vulcan XC-72R FB [19]	Cabot	254	30
Black pearls 2000 FB [19]	Cabot	1475	15
3950 FB [19]	Mitsubishi Kasei	1500	16

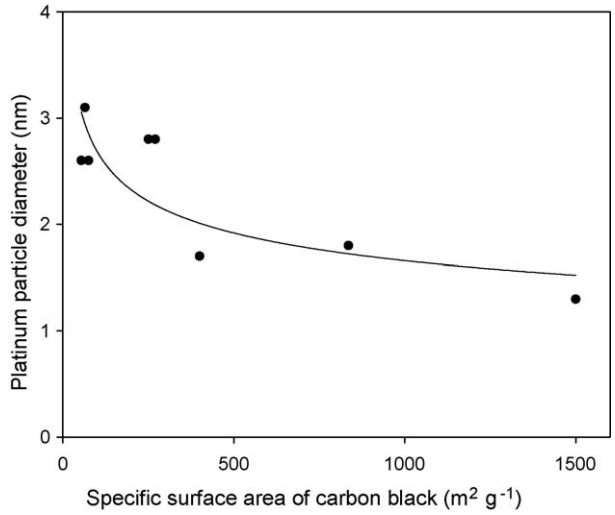

Fig. 1. Dependence of Pt particle diameter on specific surface area of carbon blacks. Reprinted from Ref. [19], copyright 1995, with permission from The Electrochemical Society.

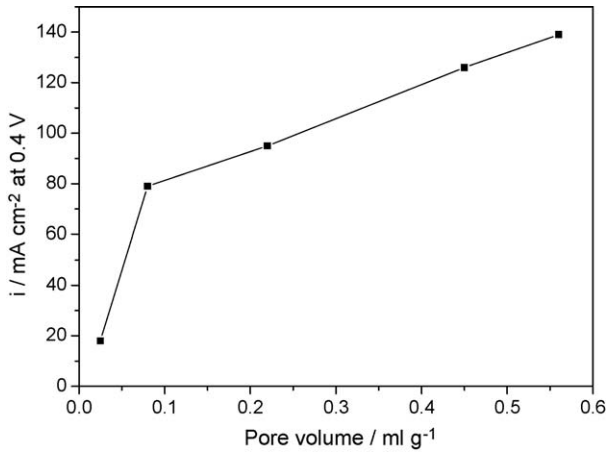

Fig. 2. Dependence of current density for methanol oxidation at 0.4 V on specific pore volume with pore diameter in the range 3–8 nm. Reprinted from Ref. [19], copyright 1995, with permission from The Electrochemical Society.

300 $m^2\ g^{-1}$ make this graphite an interesting support material for precious metal catalysts [21,22].

Graphitized carbon black is another support material of interest to catalyst manufactures. This high surface material is obtained by recrystallization of the spherical carbon black particles at 2500–3000 °C. The partially crystallized material possesses well-ordered domains. The degree of graphitization is determined by process temperature.

Many works have been devoted on the effect of carbon black characteristics on the dispersion of supported metals and on their electrocatalytic activity [19,4,23–30]. In the case of metal deposition on the carbon support by impregnation methods, the specific surface area of the carbon support seems to have only a little effect on Pt dispersion [23]. Regarding Pt/C catalysts prepared by colloidal methods, Uchida et al. [19] evaluated the effect of the specific surface area of different carbon on Pt particle size of Pt/C catalysts obtained by the sulfite-complex method. As shown in Fig. 1, Pt particle size decreased with increasing the specific surface area of carbon black. The same result was obtained by Watanabe et al. [4,24]. They observed that, notwithstanding a acetylene black supported Pt catalyst has larger Pt particle size than Pt particles supported on oil-furnace black supports, it presented higher activity for methanol oxidation. Acetylene black has a higher amount of pores with a diameter of 3–8 nm than oil-furnace black supports. As shown in Fig. 2, where the current density of methanol oxidation at 0.4 V is plotted against the volume of the pores with a diameter of 3–8 nm, the methanol oxidation increases with increasing the volume of pore with 3–8 nm size. It has to be remarked that the pores with 3–8 nm size are useful for the fuel diffusion. On the other hand, the Pt in these pores is considered not to contribute to the reaction for the PEMFC, because the particles of ionomer are larger than the pore diameters and the Pt cannot contact the ionomer. In view of that the methanol oxidation increases with increasing the volume of pores with 3–8 nm size, it means that the positive effect of these pores on fuel diffusion is greater of the negative effect on the Pt active surface area. According to the authors the pore <3 nm have no effect on methanol oxidation. This result indicates that, when the pore size is too small, supply of a fuel may not occur smoothly and the activity of the catalyst may be limited. McBreen et al. [25] investigated the dispersion of Pt deposited by a colloidal method on five carbon supports (Vulcan XC-72, Regal 600R, Monarch 1300, CSX98 and Mogul L). Vulcan XC-72 and Regal 600R presented a higher Pt dispersion than that on the other carbons. In the case of Vulcan XC-72 the high Pt dispersion was attributed to the high internal porosity, while for that regarding Regal 600R the high Pt dispersion was ascribed to the surface properties of the carbon resulting in a strong Pt-carbon interaction. Rao et al. [26] investigated carbon materials of Sibunit family prepared through pyrolysis of natural gases on carbon black surfaces as supports for the anode catalysts of direct methanol fuel cells. Specific surface area of the support varied in the wide range from 6 to 415 $m^2\ g^{-1}$. PtRu catalysts were supported on these materials by a chemical route. Comparison of the metal surface area measured by gas phase CO chemisorption and electrochemical CO stripping indicated close to 100% utilization of nanoparticle surfaces for catalysts supported on low (22–72 $m^2\ g^{-1}$) surface area Sibunit carbons. According to the authors, this high catalyst utilization could be explained by the compatibility between the size of the pores in carbon supports and Nafion® micelles. Mass activity and specific activity of PtRu anode catalysts change dramatically with the specific surface area of the support, increasing with the decrease of the latter. 10% PtRu catalyst supported on Sibunit with specific surface area of 72 $m^2\ g^{-1}$ shows mass specific activity exceeding that of commercial 20% PtRu/Vulcan XC-72 by nearly a factor of 3. The results of this work give evidence on the detrimental effect of pores with size <20 on the specific activity of PtRu/C electrocatalysts in methanol oxidation.

To compare carbon and graphite materials, Gamez et al. [27] prepared by cationic exchange PtPd catalysts supported on Vulcan XC-72R and on HSAG 300 Lonza (higher surface area graphite). The catalyst supported on Vulcan presented higher active surface area than that of the catalyst supported on HSAG.

2.1. Activation of carbon blacks

Generally, before their use as catalyst support, carbon blacks are activated to increase metal dispersion and the catalytic activity. There are two ways to activate the carbon materials: chemical activation and physical activation.

2.1.1. Chemical activation (oxidative treatment)

Derbyshire et al. [31] discovered that the surface chemistry of carbon (surface functional groups) as a result of pre-treatment is of

critical importance in determining the catalytic activity of the carbon-supported metal catalysts. The functionalities present on the carbon surface in the form of surface oxides (e.g. carboxylic groups, phenolic groups, lactonic groups, etheric groups) are responsible both for the acid/base and the redox properties of the carbon [32]. The oxidative treatment of the carbon surface gives rise to the formation of surface acidic sites and to the destruction of surface basic sites. This treatment of carbon can be performed by different oxidants: HNO_3, H_2O_2, O_2 or O_3. The effect of oxidative pre-treatment of the carbon on platinum dispersion has produced contradictory results in literature data. According to some authors [33–36], the dispersion increases with increasing the number of oxygen surface groups in the support. Torres et al. [33] showed that the effect of the different oxidants can be related to the nature of the functional groups on the carbon surface. HNO_3-treated carbon displays a high density of both strong and weak acid sites, while H_2O_2- and O_3-treated carbons show an important concentration of weak acid sites but a low concentration of strong acid sites. The H_2PtCl_6 isotherms in liquid phase at 25 °C showed a stronger interaction of the metallic precursor with the carbon of low acidity (like those treated with H_2O_2 or O_3) than with the most acidic carbon (treated with HNO_3). Carbons functionalized with weak oxidants, which develop acidic sites with moderate strength and show strong interaction with H_2PtCl_6 during impregnation, would assist the Pt dispersion on the carbon surface. According to Sepulveda-Escribano et al. [37], the presence of oxygen surface groups in the support provides for the anchoring of $[Pt(NH_3)_4]^{2+}$, but does not affect the amount of platinum retained by the support when H_2PtCl_6 is used as metal precursor. They also showed that the oxidized support hinders the reduction of the Pt precursor. Other authors [38–41], instead, reported that the presence of oxygen surface groups on carbon decreases the metal dispersion. Microcalorimetric measurements of CO adsorption performed by Guerrero-Ruiz et al. [38] evidenced that the presence of oxygen surface groups diminishes the metal-support interaction. The dependence of Pt dispersion on O_2, the total surface oxygen content of the support, is reported in Fig. 3 from Fraga et al. [23]. According to the authors, the decrease in the Pt dispersion with the increase in the total surface oxygen is due to the reduction of the number of surface basic sites, which are centres for the strong adsorption of $PtCl_6^{2-}$. The platinum content in the catalyst also depends on the oxidative treatment of carbon and decreases with increasing the more acidic surface oxygen complexes. Recently, Poh et al. [42] found that carbon materials can be easily functionalized using citric acid treatment. The citric acid treatment of the carbon surface gives rise to the formation of functional groups such as carboxyl and hydroxide. After citric acid treatment, Pt nanoparticles, deposited on functionalized Vulcan XC-72 carbon by means of a microwave-assisted polyol process, presented smaller particle size than those deposited on untreated carbon.

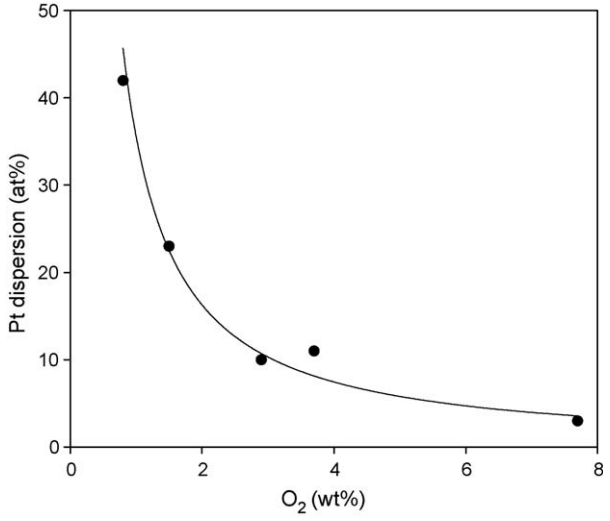

Fig. 3. Dependence of platinum dispersion in Pt/C catalysts on total surface oxygen content of the support. Reproduced from Ref. [23], copyright 2002, with permission from Elsevier.

Regarding the effect of chemical activation of the carbon on the electrocatalytic activity of supported catalysts, generally, as expected, carbon treatments, which increase metal dispersion, also increase their electrocatalytic activity [42–46]. Wang et al. [43] investigated the activity for methanol electrooxidation of Pt-Ru catalysts supported by untreated and O_3-treated Vulcan XC-72 carbon. Cyclic voltammetry in CH_3OH/H_2SO_4 solution showed that the catalytic activity for methanol oxidation of Pt-Ru catalysts supported on ozone-treated carbon is higher than that on the untreated one. Shioyama et al. [44] found that carbon black treated using C_2F_6 radio frequency plasmas is a good electrocatalyst support for PEMFC catalysts. According to the authors, the hydrophobicity of the catalyst support and the affected electronic state of the supported Pt particles, both of which are due to the introduced CF_3 group, account for the enhancement of the catalytic activity. Kim and Park [45,46] prepared carbon-supported platinum by a chemical method of H_2PtCl_6 reduction on acid/base-treated carbon blacks. The size and the loading efficiency of the metal clusters were dependent on the preparation method and the surface characteristics of the CBs. Base-treated carbon-supported Pt showed the smallest particle size of 2.65 nm and the highest loading level of 97% among the chemical-treated carbon-supported Pt catalysts. The electroactivity of the catalysts was enhanced by treatment of the carbon supports with basic or neutral agents. On the contrary, the electroactivity decayed for the acid-treated carbon-supported Pt. Gómez de la Fuente et al. [47] investigated the effect of chemical modification of Vulcan XC-72R on the activity for H_2/CO oxidation of Pt nanoparticles. They found that CO oxidation depends on the nature of the support rather than on the nature of Pt particles alone.

Recently, very interesting works focused on the functionalization of carbon support with sulfonated polymer [48] or phenyl sulfonic acid [49]. In this way the functionalized carbon plays dual roles of a mass transport and a catalyst support. The improved performance of fuel cells with the electrode containing these functionalized carbons was ascribed to a better mass transport which maximizes the catalytic activities.

A different type of functionalization is the introduction of nitrogen in the carbon structure. Indeed, recently, nitrogen-containing carbons were reported as support materials, especially in terms of well dispersion of Pt nanoparticles [50,51]. On this basis, Choi et al. [52] prepared nitrogen-doped magnetic carbon nanoparticles (N-MCNPs) by using monodispersed polypyrrole nanoparticles as the polymer precursor. Therefore, the carbonization of the polymer precursor allows generation of N-MCNPs with graphitic structures. N-MCNPs and Vulcan XC-72-supported Pt nanoparticles with metal loading of 40 wt% were synthesized by the reduction of H_2PtCl_6 using sodium borohydride as a reducing agent. TEM images of Pt/N-MCNPs (Fig. 4a), and of Pt/Vulcan XC-72 (Fig. 4b) showed that N-MCNP-supported Pt nanoparticles are more well dispersed compared to Vulcan XC-72-supported ones. Also, N-MCNPsupported Pt nanoparticles were smaller than those supported on Vulcan XC-72. In electrochemical measurement, N-MCNPs-supported Pt electrocatalysts showed higher methanol oxidation activity than Vulcan XC-72-supported one in terms of mass-normalized activity.

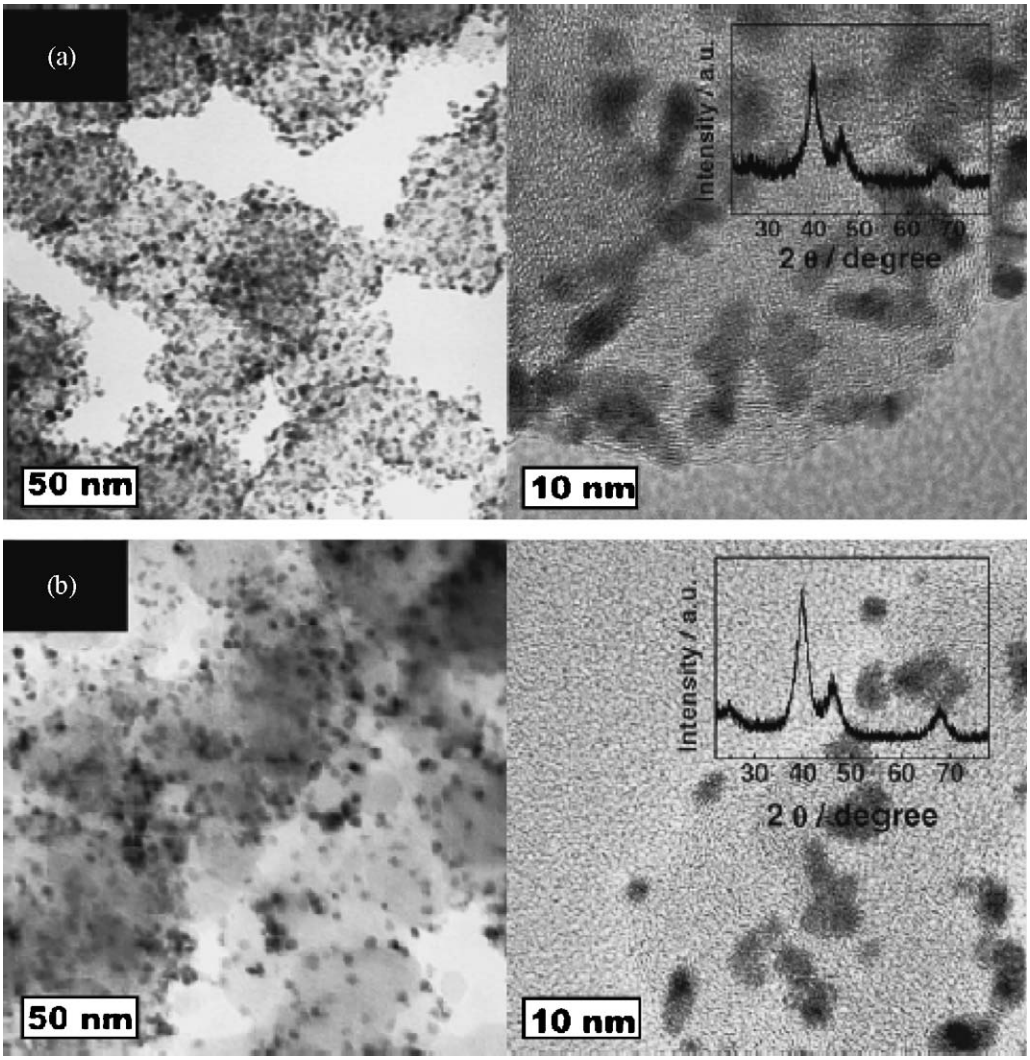

Fig. 4. Low- and high-resolution TEM images and XRD patterns of (a) Pt/N-MCNPs and (b) Pt/Vulcan XC-72. Reproduced from Ref. [52], copyright 2007, with permission from Elsevier.

2.1.2. Physical activation (thermal treatment)

The physical activation consists of a thermal treatment of the carbon performed under inert atmosphere at 800–1100 °C or in air/steam at 400–500 °C, with the aim to remove the impurities present on the carbon surface. Pinheiro et al. [53] investigated the preparation of carbon-supported Pt using three types of carbon substrates: Vulcan XC-72 powder, Shawinigan black and a fullerene soot consisting of the residue after C60/C70 fullerene extractions. Heat treatments of the carbons were carried out under two conditions: (i) argon atmosphere at 850 °C for 5 h; (ii) argon atmosphere at 850 °C for 5 h, followed by water vapour at 500 °C for 2.5 h. Following both heat treatments, from CV measurements the three carbons showed an increase of the capacitive current, due to the elimination of surface impurities. The active surface area was smaller for Pt supported on the as received Shawinigan carbon, as compared to that of Pt supported on the as received Vulcan. With the heat treatments, Pt catalysts present an increase of approximately 50% in the active surface area for both carbons. After thermal treatments of the carbons, Pt supported on the Shawinigan and fullerene substrates showed similar active areas, somewhat smaller than that of Pt supported on heat-treated Vulcan. From the Tafel plots for oxygen reduction, it was found that the catalysts supported on Vulcan and Shawinigan present similar activities, and that both are superior to the catalyst supported on fullerene carbon.

Recently Yu and Ye [54] reviewed new advances related to the physico-chemical and electronic interactions at the catalyst–support interface and to the catalyst activity enhancement through improved Pt–C interactions. They especially focused on the surface modification of the carbon support to form proper functional groups and chemical links at the platinum/carbon interface.

2.2. Stability of carbons and its effect on the stability of carbon-supported catalysts

The relation between the characteristics of carbon black materials and its effect on the stability of both the carbon support and supported metals has been investigated. The stability of carbon support affects the loss of platinum surface area following both platinum particle sintering and platinum release from the carbon support [19,24,55–57]. The relation of carbon corrosion and platinum sintering was observed from TEM analysis by Gruver [55]. McBreen et al. [24] showed that Regal 660R carbon with a low volatile content and neutral pH stabilizes platinum particles against sintering. Uchida et al. [19] tested the durability of the carbon support in sulfuric acid solution at 60 °C. The change in

color of the sulfuric acid solution is indicative of carbon support dissolution. The colors from the furnace blacks were darker than those from the acetylene blacks, and those from carbon blacks with larger surface area were darker than those from carbon blacks with smaller surface area. The furnace blacks with the larger surface area had a tendency to be more soluble and unstable. The results of X-ray fluorescence measurements indicated that few impurities are present in the acetylene blacks. Conversely, Fe, Ca, Cl and S were detected in the furnace blacks. The presence of these impurities could affect the solubility of carbon blacks.

Wang et al. [56] investigated the effect of carbon black support corrosion on the stability of Pt/C catalyst. They observed a higher oxidation degree on the Black Pearl 2000 (BP-2000) support, i.e. BP-2000 has a lower corrosion resistance than Vulcan XC-72. A higher performance loss was observed on the Pt/BP-2000 gas diffusion electrode, compared with that of Pt/Vulcan. XPS analysis suggests that higher Pt amount loss appeared in the Pt/BP-2000 after durability test. XRD analysis also shows that Pt/BP-2000 catalyst presents a higher Pt size growth. The higher performance degradation of Pt/BP-2000 is attributed significantly to the less support corrosion resistance of BP-2000. Stevens and Dahn [14] demonstrates that the thermal stability of the carbon support depends on platinum particle size, loading and temperature. They exposed a series of carbon-supported platinum electrocatalyst samples (5–80 wt% platinum deposited onto BP-2000 high surface area carbon) to temperatures in the range 125–195 °C for extended periods of time to determine their relative thermal stabilities. As expected, they found that the rate of carbon combustion increased as the platinum loading increased and as the oven temperature increased.

Antolini [8] reported the effect of the pH value during the impregnation of the metal precursor on carbon support on the Pt particle growth during thermal treatment at high temperatures. The activation energy of particle growth is lower at lower pH. It is known that the stability of the metal particles and the mechanism of platinum particle growth depend on the surface acid-base properties of the carbon support. The surface oxygen-containing functional groups may act as anchoring centres for the metal particles limiting their growth. The acidic/basic environment present on carbon surface during Pt/C impregnation with the precursor may modify the number and the characteristics of these anchoring centres, affecting in this way the movement of Pt particle on the carbon surface.

Thermal treatment stabilizes carbon against the corrosion in hot phosphoric acid [55]. Uchida et al. [19] evaluated the effect of thermal treatment at 370 °C in air or N_2 on the change from initial overpotential of methanol electrode, and on the change in catalyst content after immersion in sulfuric acid solution. Heat treatment improved the stability of the catalysts in the sulfuric acid. Following thermal treatment, the carbon support hardly dissolved in the sulfuric acid solution and the solution was transparent.

3. New carbon materials

According to the International Union of Pure and Applied Chemistry (IUPAC), pores will be classified, depending on their width, as micropores (<2 nm), mesopores (2–50 nm), and macropores (>50 nm). Generally, carbon blacks have high specific surface area but contributed mostly by micropores less than 1 nm and are therefore more difficult to be fully accessible. The presence of micropores disadvantages the carbon when used as catalyst support. Indeed, when the average diameter of the pores is less than 2 nm, supply of a fuel may not occur smoothly and the activity of the catalyst may be limited. Moreover, it is known that micropores of these types of amorphous carbon particles are poorly connected. Compared with carbon blacks, generally mesoporous carbons (MCs) presented higher surface area and lower amount or absence of micropores. In a mesoporous carbon-supported catalyst, the metal catalyst particles are distributed and supported on the surface or in pores of the mesoporous carbon. A large mesopore surface area, particularly with pore size >20 nm, gives rise to a high dispersion of Pt particles, which resulted in a large effective surface area of Pt with a high catalytic activity. The mesoporous structure facilitated smooth mass transportation to give rise to high limiting currents.

Recent studies have revealed that the physical properties of the carbon support can greatly affect the electrochemical properties of the fuel cell catalyst [29,58–65]. It has been reported that carbon materials with both high surface area and good crystallinity can not only provide a high dispersion of Pt nanoparticles, but also facilitate electron transfer, resulting in better device performance [29,58]. On this basis, novel non-conventional carbon materials have attracted much interest as electrocatalyst support because of their good electrical and mechanical properties and their versatility in pore size and pore distribution tailoring. These materials present a different morphology than carbon blacks both at the nanoscopic level in terms of their pore texture (for example mesopore carbon) and at the macroscopic level in terms of their form (for example microsphere). The examples are supports produced from ordered mesoporous carbons (OMCs), carbon aerogels, carbon nanotubes (CNTs), carbon nanohorns (CNHs), carbon nanocoils (CNCs) and carbon nanofibers (CNFs).

These new carbon materials can be prepared in form of microspheres, as in the case of ordered mesoporous carbons, using spherical templates [66] and carbon gels [67], or can grow directly on the surface of carbon [68], polymeric [69] or metal [70] microspheres, as in the case of carbon nanotubes. Carbon microspheres (CMSs) can be prepared by template method [66], sol–gel method [67], ultrasonic spray pyrolysis (USP) [71,72] and hydrothermal method [73,74]. The diameter of carbon microspheres is about 1–2 μm, i.e. considerably higher than the diameter of CBs. Fig. 5 from Ref. [71] shows SEM micrographs of carbon microspheres prepared by USP and of Vulcan XC-72R carbon powder. While the USP process facilitates spherical particle formation, the internal pore structure is formed during the precursor decomposition. In PC-I (formed from USP of a lithium dichloroacetate solution), interconnected mesopores are observed within the individual carbon spheres, as shown in Fig. 5a. In the case of PC-I, precursor melting comes firstly, and then decomposition follows [72], leading to formation of mesopores in carbon spheres. PC-I spheres are largely distributed in the 1–2 μm region. Resistivity measurements indicated that that PC-I is a poor conductor as compared to Vulcan XC-72. In PC-II (formed from USP of a sodium chloroacetate solution), on the contrary, large macropores are present (Fig. 5b), which generates a much more open carbon network. In PC-II (unlike PC-I), no melting occurs before precursor decomposition; as a result, the carbon network forms through solid-state reactions, resulting in macropore formation [72]. Finally, the SEM of the Vulcan XC-72 carbon (Fig. 5c) shows a very different morphology compared to that of the two USP carbons. The Vulcan carbon is composed of nanosized carbon particles, extensively agglomerated, with micropores only. Good metal dispersion on CMS than on CB is generally observed [71,73,74]. Bang et al. [71] compared the performance of DMFCs with PtRu supported on CMS and Vulcan. PtRu/Vulcan showed a slightly higher performance than that of PtRu/CMS in the activation-controlled region (low current density region): this is likely due to relatively low connectivity between carbon networks in the PtRu/CMS catalyst, which leads to poor conductivity. The activity for methanol oxidation of PtRu/Vulcan in the mass

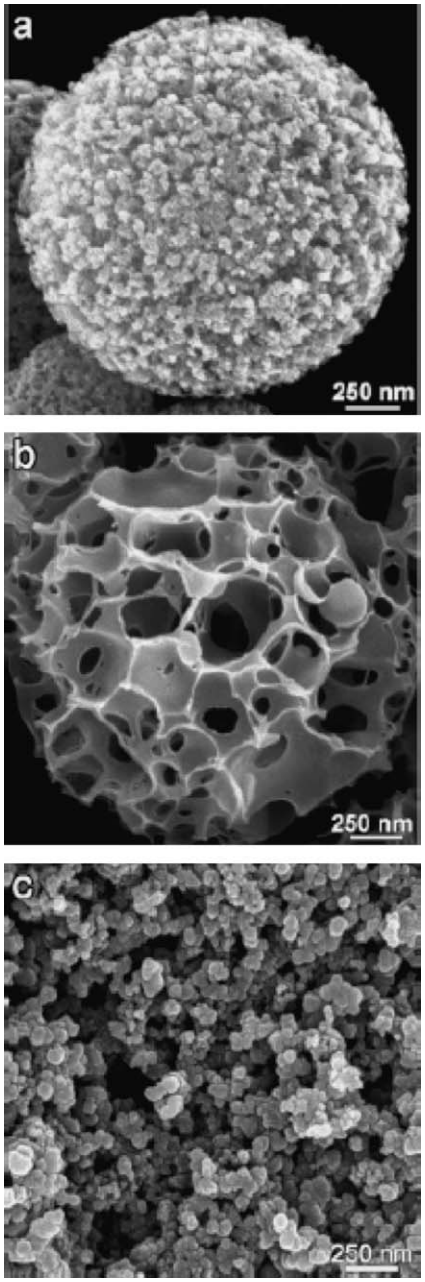

Fig. 5. SEM micrographs of (a) PC-I, (b) PC-II, and (c) Vulcan XC-72. Reproduced from Ref. [71], copyright 2007, with permission from the American Chemical Society.

transport-controlled region (high current density region), instead, was lower than that of PtRu/CMS: indeed, PtRu/CMS provides more space in the membrane electrode assembly (MEA), due to the micrometer-sized spheres. The increased inter-particle voids help to prevent flooding of the electrode caused by water and blocking of the mass transport channels by carbon dioxide bubbles produced during the unit cell operation and result in a better performance in the high current density region. The larger particle size of CMS results in lower electrical conductivity and improved mass transport than CB Vulcan.

Also hard or hollow carbon spheres (HCSs) represent promising macroscopic forms of these new carbon materials. Yang et al. [75] used monodispersed hard carbon spherules, prepared by hydrothermal method with sugar as the precursor, as a support of Pt nanoparticles. HCS particles were monodispersed with an average diameter of ca. 2 μm. Pt supported on hard carbon spherules exhibited a higher catalytic activity in the electrooxidation of methanol than either the Pt/CMS or the commercial Pt/Vulcan XC-72 catalyst. Wen et al. [76] prepared hollow carbon spheres by pyrolysis of hollow carbonaceous composites at 900 °C under nitrogen flow. Pt nanoparticles were uniformly anchored on the outer and the inner surface of HCSs. Hollow carbon sphere supported Pt electrode showed significantly higher electrocatalytic activity and more stability for methanol oxidation compared with carbon microspheres supported Pt and commercial Pt/Vulcan XC-72 electrodes. According to the authors, the excellent performance of the Pt/HCS might be attributed to the high dispersion of platinum catalysts and the particular hollow structure of HCSs. Fang et al. [77] prepared spherical carbon capsules with a hollow macroporous core of ca. 280 nm and a ca. 40 nm thick mesoporous shell. They observed a considerable improvement in electrocatalytic activity towards oxygen reduction reactions and in fuel cell performance by using Pt supported on these carbon capsules when compared with Pt supported on carbon black Vulcan XC-72.

The characteristics of some new carbon materials, metal dispersion and the electrochemical activity of catalysts supported on these materials, compared with those of catalysts supported on carbon blacks, are reported in the following paragraphs.

3.1. Mesoporous carbons

3.1.1. Ordered mesoporous carbons

3.1.1.1. Preparation methods and structural characteristics. The ordered mesoporous carbons have recently received great attention because of their potential use as catalytic supports in fuel cell electrodes. They have controllable pore sizes, high surface areas and large pore volumes [66,78]. Nanoporous carbons with 3D-ordered pore structures have been shown to improve the mass transport of reactants and products during fuel cell operation [78,79]. Ordered mesoporous carbons have recently been synthesized using ordered mesoporous silica templates [80]. The synthesis procedure involves infiltration of the pores of the template with appropriate carbon precursor (furfuryl alcohol, sucrose, acenaphthene and mesophase pitch, etc.), its carbonization, and subsequent template removal. The resultant carbon depends on the structure of the template. The template needs to exhibit three-dimensional pore structure in order to be suitable for the ordered mesoporous carbon synthesis, otherwise disordered microporous carbon is formed. MCM-48, SBA-1 and SBA-15 silicas were successfully used to synthesize carbons with cubic or hexagonal frameworks, narrow mesopore-size distributions, high nitrogen BET specific surface areas (up to 1800 $m^2\ g^{-1}$), and large pore volumes. Chang et al. [81] reviewed the synthesis and application aspects of ordered mesoporous carbon as a novel material for fuel cell catalysts. There are various types of ordered mesoporous carbons. The most tested as fuel cell catalyst support is the ordered CMK-3 carbon. The first ordered mesoporous carbon that was a faithful replica of the template was synthesized by Jun et al. [82] using SBA-15 silica [83] as a template. The ordered structure of the CMK-3 carbon, obtained by Jun et al. [82] using SBA-15 silica as the template, sucrose as the carbon source, the triblock copolymer Pluronic P123 as the surfactant and tetraethylorthosilicate (TEOS) as the silica source, is exactly an inverse replica without involving structural transformation during the removal of the silica template. This material consists of uniformly sized carbon rods arranged in a hexagonal pattern. CMK-3 synthesized by Jun et al. [82] exhibited large adsorption capacity, with a nitrogen BET specific surface area of about 1500 $m^2\ g^{-1}$ and total pore volume of about 1.3 $cm^3\ g^{-1}$. CMK-3 has a primary pore

size of about 4.5 nm, accompanied by micropores and some secondary mesopores. As previously reported, the pores with 3–8 nm size are useful for the fuel diffusion, but the Pt in these pores is considered not to contribute to the reaction for the PEMFC, because the particles of ionomer are larger than the pore diameters and the Pt cannot contact the ionomer. On this basis, the mesoporous carbon obtained by Jun et al. [82] is not suitable for the use in fuel cells. The pore-wall thickness of SBA-15, however, can be readily tailored: this feature is promising for the point of view of CMK-3 pore-size tailoring. CMK-3 can be obtained when the SBA-15 template is calcined at 880 °C prior to carbon precursor infiltration. This calcination procedure, however, leads to a large structural shrinkage and to significant depletion of the micropores and small mesopores that are responsible for the connectivity between the SBA-15 large pore channels [84]. In contrast, SBA-15 calcined at somewhat higher temperature (970 °C) afforded disordered carbon [84]. The methods developed for the synthesis of ordered mesoporous carbons are simple and not too expensive [85]. CMK-3 carbon is particularly promising because of the fact that SBA-15 template is inexpensive [86] and easy to synthesize [85], and its pore-wall thickness can be readily tailored. TEM images of CMK-3 are shown in Fig. 6 from Ref. [87]. Fig. 6a and b indicates that the structure of CMK-3 is highly ordered. The images were recorded along two different crystallographic directions, showing the typical features of CMK-3. The structure is an inverse replica of the structure of SBA-15 silica used as template.

Suitable carbon supports for fuel cell catalysts have to combine a good electronic conductivity with a large and accessible surface area. However, materials with these characteristics are difficult to synthesize. In particular, ordered mesoporous carbons obtained using a SBA-15 hard-template possess low conductivity (0.3×10^{-2} S cm^{-1} [88]), due to the poor contribution of carbon connections among the rope-like particles. This problem can be overcome by two ways, (a) preparing graphitizable carbons [89], and (b) using SBA-15 powder [90]. Fuertes and Alvarez [89] synthesized graphitizable carbons by the infiltration of the porosity of mesoporous silica with a solution containing the carbon precursor (i.e. polyvinyl chloride, PVC), the carbonization of the silica–PVC composite and the removal of the silica skeletal. Carbons obtained in this way have a certain graphitic order and an improved electrical conductivity (0.3 S cm^{-1}), which is two orders larger than that of a non-graphitizable carbon. Wang et al. [90] prepared a highly ordered mesoporous carbon from the template of SBA-15 powder. The mesoporous carbon monolith exhibited superior conductivity (1.37 S cm^{-1}) compared with mesoporous carbon monolith synthesized from SBA-15 monolith. According to the authors, the good conductivity of these MCs is reasonably attributed to the major contribution of carbon connections among the rope-like particles. Possibly, the connecting carbon in acts as the skeleton, which is favourable for the good conductivity.

The synthesis method based on the use of a hard-template involve multiple steps consisting of preparation of the rigid template separately followed by infiltration of the pores of the template with an appropriate carbon precursor and subsequent carbonization and removal of the template. Also, although effort has been made to control the pore diameter in the carbon by controlling the pore-wall thickness of the template, the control of pore diameter remains a challenge. Alternative methods to prepare ordered mesoporous carbon are the colloidal template route (soft-template synthesis) [91,92] and the structure-directing agent/surfactant synthesis [93–95]. Raghuveer and Manthiram [91,92] synthesized mesoporous carbons with high surface area (500–990 m^2 g^{-1}), large pore diameter, and enhanced mesoporosity by a soft colloidal template route with various aniline/cetyltrimethylammonium bromide (CTABr) ratios. The soft colloidal template route allows control of the porosity of the mesoporous carbons by tuning the geometry of the colloidal silica template via a variation of the aniline/CTABr ratios in the colloidal composition. Surfactant-stabilized silica particle templates were first obtained by dissolving the surfactant CTABr in water followed by an addition of tetraethylorthosilicate and HCl. Then, required amounts of the swelling agent aniline and the polymerization initiator ammonium peroxodisulfate were added to the colloidal solution. The aniline/CTABr ratio was varied from 0 to 0.7 in order to obtain mesoporous carbons with various porosities. The broad pore distribution (10–40 nm) was presented by the sample prepared with an aniline/CTABr ratio of 0.2. The latter method is based on a commercially available triblock copolymer (Pluronic F127) as a structure-directing agent and a mixture of resorcinol/formaldehyde or phloroglucinol/formaldehyde as a carbon precursor under mild and widely variable processing conditions [93–95]. Liang and Daí [93] synthesized highly ordered mesoporous carbon structures based on Pluronic F127 as a structure-directing agent and a mixture of phloroglucinol and formaldehyde as an inexpensive

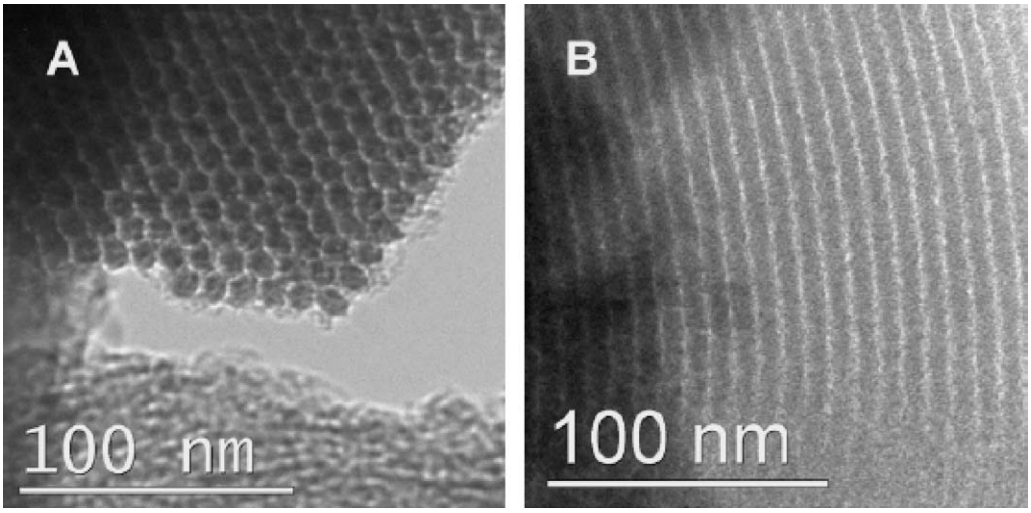

Fig. 6. TEM images of CMK-3 carbons. (a) Hexagonal structure of CMK-3 carbon, (b) parallel mesopores of CMK-3 carbon. Reproduced from Ref. [87], copyright 2007, with permission from Elsevier.

carbon precursor. They used phloroglucinol as it polymerizes much faster than either resorcinol or phenol. The polymer phase was subsequently processed in three different ways to produce the mesoporous carbons with monolith, fiber, and film morphologies, which were denoted as Mon-C-g, Fiber-C-g, and Film-C-g, respectively. The BET surface areas of Mon-C-g, Fiber-C-g, and Film-C-g are 377.9, 593.0, and 569.1 $m^2 g^{-1}$ and the corresponding average pore sizes are 9.5, 6.1, and 5.4 nm, respectively. In conclusion, phloroglucinol was found to be an excellent precursor for the synthesis of mesoporous carbons when commercially available triblock copolymers were used as structure-directing agents.

Ordered mesoporous carbons contain a small amount of oxygen surface groups, which is disadvantageous for many applications. We previously reported the relevance of the functionalization of carbon supports on the dispersion and anchoring of platinum particles on the support. The functionalization of OMC has not been studied in a large extent because their ordered structure could collapse during the process. Ryoo et al. [96] reported that ordered mesoporous carbons can maintain an ordered structure even in boiling 5 M aqueous solution of NaOH, KOH, or H_2SO_4 over a week, showing strong resistance to attack by acids and bases. Before deposition of platinum, Calvillo et al. [87] modified the texture and surface chemistry of the support by oxidation treatments in liquid phase using nitric acid as oxidative agent. During the oxidation process, oxygen surface groups were created, whereas the ordered porous structure was maintained.

3.1.1.2. Metal dispersion and electrochemical properties. Ordered mesoporous carbons have been tested as support for fuel cell catalysts, and their metal dispersion and catalytic activity has been compared with that of catalysts supported on carbon blacks. Generally, all OMC supported metals presented higher metal dispersion and higher catalytic activity, both for oxygen reduction and methanol oxidation, than CB supported metals.

Joo and co-workers [66] described a general strategy for the synthesis of highly ordered, rigid arrays of nanoporous carbon having uniform but tunable diameters (typically 6 nm inside and 9 nm outside). The resulting material supports a high dispersion of platinum nanoparticles, exceeding that of other common microporous carbon materials. The platinum cluster diameter can be controlled to below 3 nm, and the high dispersion of these metal clusters gives rise to promising electrocatalytic activity for oxygen reduction. Ding et al. [97] prepared CMK-3 ordered carbon using SBA-15 as template. CMK-3 supported Pt and Pt-Ru nanoparticles were tested for oxygen reduction and methanol oxidation reactions, respectively. The ORR activity of the Pt/CMK-3 catalyst was higher than that of a commercial catalyst. Conversely, the Pt-Ru/CMK-3 catalyst was not effective for methanol oxidation. Joo et al. [98] prepared two OMC samples with hexagonal mesostructure from phenanthrene and sucrose by nano-replication method using mesoporous silica as a template. Structural characterizations revealed that both OMCs exhibited large BET surface area and uniform mesopores, while the OMC synthesized from phenanthrene exhibited lower sheet resistance than the OMC derived from sucrose. The Pt nanoparticles were supported on both OMCs with very high dispersion, as the particle size was estimated under 3 nm despite high metal loading of 60 wt%. In single DMFC test, the OMC supported Pt catalysts exhibited much higher performance than the commercial catalyst, which may be attributed to the high surface area and uniform mesopore networks of OMC. Su et al. [79] prepared ordered graphitic mesoporous carbon (GMC) by chemical vapour deposition (CVD) of benzene in the pores of mesoporous SBA-15 pure-silica template without loading any catalytic species. The catalytic performance of the mesoporous carbon-supported Pt catalyst in room-temperature methanol oxidation was higher than that of a commercial Pt catalyst from E-TEK. As previously reported, Calvillo et al. [87] prepared functionalized OMC with a specific area of 570 $m^2 g^{-1}$. An OMC supported Pt electrocatalyst was prepared by the impregnation method followed by reduction of Pt precursor with sodium borohydride. Fig. 7 shows TEM images of platinum supported on functionalized CMK-3. According to the authors, platinum was well dispersed over the functionalized mesoporous support and its catalytic performance towards methanol oxidation improved when compared with carbon Vulcan XC-72. By an accurate observation of Fig. 7, however, it results the presence of some particle agglomeration. The better performance of the OMC supported catalyst, notwithstanding the presence of some particle agglomeration, was due to higher amount of mesopores in the support, aiding the reactant flow.

Yamada et al. [99] synthesized OMCs by a colloidal-crystal templating method. The porous carbon showed a large surface area with monodispersed three-dimensionally interconnected mesopores (45 nm). A large mesopore surface area prompted dispersion of Pt particles, which resulted in a large effective surface area of Pt

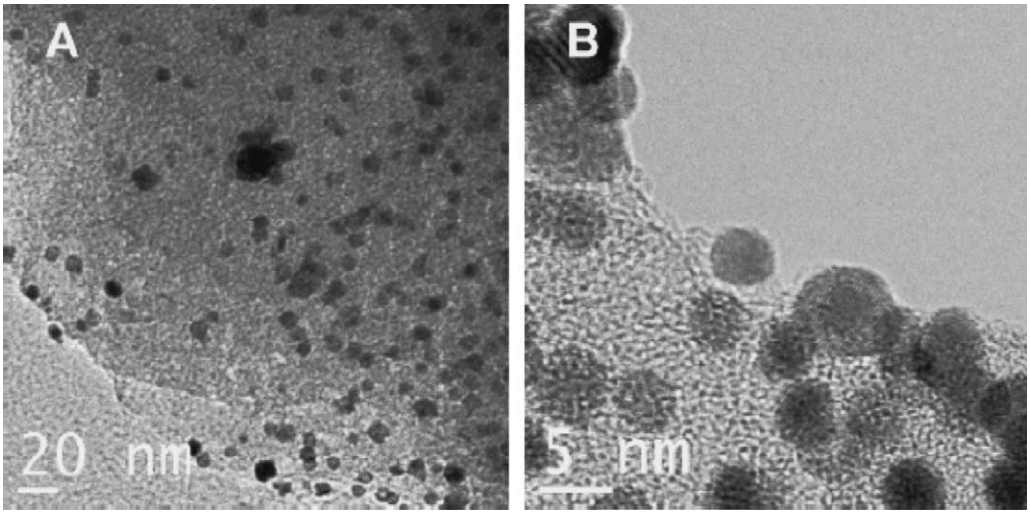

Fig. 7. TEM images of platinum supported on functionalized CMK-3. Reproduced from Ref. [87], copyright 2007, with permission from Elsevier.

with a high activity for the oxygen reduction reaction. The porous structure facilitated smooth mass transportation to give rise to high limiting currents.

Raghuveer and Manthiram [91] prepared Pt catalyst supported on mesoporous carbons, obtained by soft-template route, by adding a required amount of hexachloroplatinic acid to the mesoporous carbon, followed by reduction in H_2 at 550 °C for 2 h. The mesoporous carbons loaded with Pt catalysts exhibited three times higher mass activity for methanol oxidation than the Vulcan XC-72R. The enhanced activity is due to the better dispersion and utilization of the Pt catalysts, which originate, respectively, from a higher surface area and the absence of micropores (enhanced mesoporosity). Vengatesan et al. [100] synthesized mesoporous carbons using soft colloidal template route. Supported Pt catalysts were prepared by aqueous impregnation using synthesized mesoporous carbon as well as commercial Vulcan carbon. The electrochemically active surface area (ECSA) of the Pt/MC catalyst was higher than that of the Pt/Vulcan catalyst at the same Pt loading. This indicated the higher activity of the Pt/MC catalysts towards electrochemical reaction, due to high dispersion of the Pt particles.

Hayashi et al. [101] prepared mesoporous carbons using Pluronic F127 as a structure-directing agent and a mixture of resorcinol/formaldehyde as a carbon precursor. When mesoporous carbon-supported Pt was synthesized using platinum(II) acetylacetonate, Pt particles were well dispersed on MC. Pt/MC showed a clear hydrogen adsorption/desorption peak even though it was much smaller than Pt/CB. Since Pt-surface area is comparative between Pt/MC and Pt/CB, the authors concluded that some Pt particles were in the mesopores and not involved in hydrogen adsorption. However, all the Pt including inside and outside the pores was in use for oxygen reduction.

3.1.2. Carbon gels

3.1.2.1. Preparation methods and structural characteristics. Carbon gels have recently attracted attention as a new form of mesoporous carbon. Their surface area, pore volume, and pore-size distribution are tunable surface properties related to the synthesis and processing conditions, which can produce a wide spectrum of materials with unique properties [102]. These materials have a great versatility both at the nanoscopic level in terms of their pore texture and at the macroscopic level in terms of their form (for example microsphere, powder or thin film). Generally, carbon gels are obtained from the carbonization of organic gels, which are prepared from the sol–gel polycondensation of certain organic monomers. The are three type of carbon gels, depending on the synthesis method: carbon aerogels, carbon xerogels and carbon cryogels. Their synthesis method only differs in the way of drying. Carbon gels are commonly synthesized through the sol–gel polycondensation of resorcinol [$C_6H_4(OH)_2$] and formaldehyde (HCHO) (R/F) in a slightly basic aqueous solution, followed by drying and pyrolysis in an inert atmosphere. In general, an aerogel is produced when the solvent contained within the voids of a gelatinous structure is exchanged with an alternative solvent, such as liquid CO_2, that can be removed supercritically in the absence of a vapour–liquid interface and thus without any interfacial tension [103]. Ideally, this supercritical drying process leaves the gel structure unchanged with no shrinkage of the internal voids or pores [104]. The supercritical drying process, however, makes carbon aerogels quite expensive. In contrast, a xerogel is produced when the solvent is removed by conventional methods such as evaporation under normal, nonsupercritical conditions. This typical drying process causes the internal gel structure to collapse because of the tremendous interfacial tension caused by the presence of the vapour–liquid interface, especially in the very small voids or pores [104]. Finally, mesoporous carbons with narrow pore-size distribution can be obtained by the less expensive and safer procedure such as freeze drying, the corresponding carbons being called cryogels [105]. Zanto et al. [106] compared the effect of synthesis parameters, such as gel pH, weight percentage of solids and pyrolysis temperature, on carbon aerogels and carbon xerogels. On average, the carbon aerogels exhibited higher surface areas and pore volumes than the carbon xerogels. The highest surface area and the highest pore volume for carbon aerogels were 929 $m^2\ g^{-1}$ and 1.42 $cm^3\ g^{-1}$, respectively. The corresponding values for the carbon xerogels were 591 $m^2\ g^{-1}$ and 0.44 $cm^3\ g^{-1}$, and were obtained under completely different conditions. In general, the properties of the carbon aerogels were more sensitive to the synthesis and processing conditions than the carbon xerogels. This indicates that carbon aerogels might be more tunable to a specific application than carbon xerogels. In this work, however, it was not reported the relative amount of micro-, meso- and macropores. The pore distribution, particularly the amount of mesopores, is essential for the use of these materials in fuel cells. The support must possess high mesoporosity in the pore-size range of 20–40 nm for a high accessible surface area. Indeed, the Nafion binder solution, which is generally used in electrode preparation, is constituted by ionomers that may occlude pores narrower than 20 nm, so that catalyst particles chemically deposited in such pores are not in contact with the proton conductor and the fuel. Marie et al. [107] prepared two carbon aerogels from resorcinol (R)–formaldehyde (F) sol with F/R = 2 molar ratio. The gelation catalyst (C) was sodium carbonate. The reactant molar ratios (R/C) were 200 (CA1) and 300 (CA2). CA2 presented a higher BET surface area than the CA1, due to a higher microporous volume. CA1 had the largest part of its porous volume (4.8 $cm^3\ g^{-1}$) made up of pores in the mesoporous range (34 ± 4 nm). In the case of CA2, instead, no significant contribution to the porous volume is found in the mesopore range. The full porous volume of CA2 (5.6 $cm^3\ g^{-1}$) is essentially constituted of pores larger than 50 nm, in the 50–66 nm range. Job et al. [108] produced resorcinol–formaldehyde xerogels at various temperatures (50, 70 and 90 °C) and with three different R/C ratios (500, 1000 and 2000). The effect of these variables was studied in order to optimize the synthesis conditions. Both the pore size and pore volume depend on the synthesis temperature, especially when R/C is high: the pore size tends to decrease when the synthesis temperature increases but this can be counterbalanced by increasing the R/C ratio (i.e. by decreasing the pH of the precursors solution). As a rule, both the pore size and pore volume increase when R/C increases. For R/C = 500 the maximum pore size ($d_{p,max}$) is in the range from 10 to 26 nm, for R/C = 1000$d_{p,max}$ goes from 17 to 80 nm, and for R/C = 2000$d_{p,max}$ goes from 60 to 600 nm.

Carbon cryogels possess high BET surface areas and large mesopore volumes because of their uniform mesopores formed among the unique network structure [109–113]; therefore, they are suitable for application as new carbonaceous supporting materials. Their mesoporosity could be controlled by varying the amount of catalyst used in the sol–gel polycondensation [109,114]. Furthermore, Kim et al. [115] have recently reported that the mesopore size and the particle size of carbon cryogel microspheres could be controlled simultaneously by adjusting the concentration of the nonionic surfactant used in the inverse emulsion polymerization.

3.1.2.2. Metal dispersion and electrochemical properties of carbon gels. Moreno-Castilla et al. [102] reviewed the preparation of metal-doped carbon aerogels, their physico-chemical surface properties and their applications as catalysts in various reactions. There are few works dealing on the electrocatalytic

properties of gel supported catalysts for use in low-temperature fuel cells. Kim et al. [67] investigated the preparation of highly dispersed platinum nanoparticles on carbon cryogel microspheres. The Pt nanoparticles were loaded on carbon cryogels using a wet impregnation method. Supported catalysts with a low Pt loading of 1.2 wt% showed high metal dispersions (over 33%). The Pt particle size was in the range 2.7–3.4 nm. The Pt particle size increased up to 17.7 nm for a Pt loading of 10 wt%. They did not investigate, however, the behaviour of these catalysts in fuel cell. Kim et al. [116] synthesized polymer–silica composites by resorcinol–formaldehyde polymerization in the presence of uniform size silica particles. After carbonization and subsequent removal of the silica template, these polymer–silica composites turned into nanoporous carbon xerogels with high surface area and large pore size. By controlling the initial pH of the carbon precursor solution, they prepared nanoporous carbon xerogels with different textural properties. For DMFC application, a PtRu alloy was supported on carbon xerogels and activated carbons by a formaldehyde reduction method [117]. They found that the textural properties of carbon supports play important roles in the metal dispersion and DMFC performance of the supported PtRu catalysts. The support with large pore size and high surface area (especially, meso-macropore area) was favourable for high dispersion of the PtRu catalyst and easy formation of triple-phase boundary. Microporous framework, resulted from the destruction of structural integrity, was insufficient for high dispersion of PtRu species. The catalysts with higher metal dispersion and structural integrity showed higher catalytic activities in the methanol electro-oxidation and the DMFC performance test. Babić et al. [118] investigated the kinetics of hydrogen oxidation reaction in perchloric acid solution on carbon-supported Pt nanoparticles using the rotating disk electrode technique. Carbon cryogel and carbon black Vulcan XC-72 were used as catalyst supports. Supported Pt catalysts were prepared by a modified polyol synthesis method in an ethylene glycol solution. They found that Pt catalyst prepared by using carbon cryogel as support presents higher hydrogen electrochemical oxidation activity than the catalyst prepared by using Vulcan XC-72. Arbizzani et al. [119] prepared two carbon cryogels, named CC1 and CC2, with pore-size distribution centred at 6 and 20 nm, respectively, by sol–gel R/F polycondensation. Electrodeposited PtRu on CC2-Nafion support with ca. 0.1 mg Pt cm^{-2} displayed a good catalytic activity for methanol oxidation of 85 mA mg^{-1} Pt after 600 s at 492 mV vs. NHE and 60 °C in H_2SO_4 0.1 M/CH_3OH 0.5 M. The catalytic activity tests and XRD and SEM analyses demonstrated the stability of the prepared electrodes upon catalysis in the time scale of the measurements. The same authors [120] prepared mesoporous cryo- and xerogel carbons, and investigated the catalytic activity of PtRu catalysts chemically and electrochemically deposited on such carbons. Cryo- and xerogel carbons presented higher specific total volume and surface area and, more importantly, higher mesoporosity than that of Vulcan. The carbon featuring the highest mesoporosity was the C5.7-500 cryogel (prepared using a dilution factor, i.e. the water to gel precursors molar ratio, and a resorcinol to gelation catalyst molar ratio of 5.7 and 500, respectively), which exhibits 1.35 cm^3 g^{-1} and 285 m^2 g^{-1} meso-macropore specific volume and surface area, respectively, and such values increase by 20% after activation at 400 °C. The specific activity for methanol oxidation of carbon-supported PtRu increased more than double when Vulcan is substituted by cryo- and xerogel carbons. For 21–24% Pt loading on carbon the highest catalytic activity is reached with the PtRu/C5.7-500 electrode featuring the carbon support with the highest area developed from the pores >20 nm, which provide the best proton and fuel transport in the catalyst layer. The authors explained the better performance provided by cryo/xero carbon supports with respect to Vulcan by considering that they feature a high specific surface area from pores wider than 20 nm which may guarantee a better contact among the PtRu, the fuel and the electrolyte. Guilminot et al. [121] developed new nanostructured carbons through pyrolysis of organic aerogels, based on supercritical drying of cellulose acetate gels. These cellulose acetate-based carbon aerogels are activated by CO_2 at 800 °C and impregnated by $PtCl_6^{2-}$; followed by chemical or electrochemical reduction of Pt. The oxygen reduction reaction kinetic parameters of the carbon aerogel supported Pt, determined from quasi-steady-state voltammetry, were comparable with those of Pt/Vulcan XC-72R. Du et al. [122] prepared a carbon aerogel supported Pt-Ru catalyst. The direct methanol fuel cell with this catalyst as anode material attained a good performance. The authors ascribed the advantages of the use of carbon aerogel as catalyst support to the mesopore structure that can facilitate the mass transportation in the electrode. Marie et al. [107] compared two carbon aerogels with different nanopore-size distributions but both with high surface area, high nanoporous volume and low bulk density as platinum support. The platinum was deposited on the carbon by means of two different techniques, one employing an anionic platinum precursor, the other using a cationic one. The structural differences between the carbon aerogels did not yield any difference in platinum deposits in terms of Pt-surface area and ORR activity. According to the authors, the similarity of the platinum deposit kinetic activity on the two carbon aerogels further will allow in future work to make new catalytic layers based on Pt-doped carbon aerogels with different structures but identical platinum deposit in terms of surface area and intrinsic activity. This should be beneficial in studying the structural improvements (pore-size distribution optimization) of new PEMFC catalytic layers based on carbon aerogels. Conversely, the ORR mass activity of the high Pt-surface area samples, obtained by the cationic insertion technique, leading to the oxidation of carbon gel surface (oxCA), was several times lower than that of the samples obtained by the anionic technique. This result could be ascribed to: (1) the size of platinum particles being too small on Pt/oxCA samples (negative particle-size effect); (2) the platinum particles, due to their smallness, being located more deeply in the porous network of the carbon aerogel, which implies a more difficult access to oxygen and thus a decrease in the ORR performance. According to the authors, it is more probable that the low activity of the Pt/oxCA catalysts is mainly due to the platinum particle-size effect. The same research group [123] compared the electrochemically active area of Pt supported on a carbon aerogel with that of Pt supported on Vulcan. Pt-doped Vulcan exhibited higher active area. This result is somewhat surprising considering the lower specific BET surface area of Vulcan XC-72 (about 200 m^2 g^{-1}) compared to the carbon aerogel (about 1000 m^2 g^{-1}). Moreover, this measurement does not agree with the TEM micrographs, which show smaller platinum particles (2–5 nm) supported on the carbon aerogel than on the carbon black. They estimate that about 75% of the geometrical surface area of the Pt particles is electrochemically active for the E-TEK material, and less than 25% for carbon aerogel. In summary, Pt particles are very well distributed on the carbon aerogel, but most of it is electrochemically inactive. The carbon aerogel shows interesting ORR kinetic parameters in term of specific activity, but the lower accessibility of the platinum particles on carbon aerogel than on Vulcan XC-72 lowers its mass activity. One possibility is that the surfaces of the nanoparticles are occluded by being partially

buried in pores or irregularities on the carbon surface and are only partially wetted by the liquid electrolyte. In a PEMFC, this issue might be even more drastic, as the electrolyte will not be a liquid but a polymer, and hence less prone to wet easily the active layer. This result shows the great importance of the carbon pore size/metal particle-size ratio. Indeed, the metal particles can be distributed and supported on the surface or in pores of the mesoporous carbon. Depending on this ratio the metal particles can:

(1) not enter into the pores (active metal particles);
(2) enter into the pores, but Nafion binder does not enter or obstructs the carbon's mesopores (inactive metal particles);
(3) enter into the pores, and Nafion binder also enter without obstruct the carbon's mesopores and its presence in the composite only decreases the pore volume (active metal particles).

Regarding the stability of the MCs in fuel cell conditions, due to their low degree of graphitization, very similar to that of carbon black, they suffer corrosion problems. Graphitized carbon black supports with the same surface area and platinum loading as ungraphitized supports showed much greater stability under fuel cell conditions [15]. The graphitization of the MCs derived from hard-template synthesis at high temperature (>2000 °C) can lead to the collapse of the corresponding mesostructures because of their intrinsic absence of strong pore-wall structures. The pore-walls of these MCPs are held together through thin carbon filaments. Unlike the MCs derived from a hard-template, the MCs derived from a soft-template entail strong pore-wall structures. They are expected to retain their mesostructures and associated surface area under severe graphitization conditions, leading to graphitic mesoporous carbons with considerably enhanced chemical stability. Shanahan et al. [124] prepared GMCs and carried out extended corrosion experiments on GMC and Vulcan supported Pt by chronoamperometric measurements in H_2SO_4 for 160 h. The Pt/Vulcan showed a 39% loss in catalytic surface area, while the Pt/GMC exhibited an initial gain and finally a 14% loss in catalytic surface area, indicating that GMC could potentially provide much higher durability than Vulcan XC-72.

3.2. Carbon nanotubes

3.2.1. Preparation methods and structural characteristics

The tubular structure of carbon nanotubes makes them unique among different forms of carbon, and they can thus be exploited as an alternative material for catalyst support in heterogeneous catalysis [125] and in fuel cells due to the high surface area, excellent electronic conductivity, and high chemical stability [126–135]. Conventional carbon nanotubes are made of seamless cylinders of hexagonal carbon networks and are synthesized as single-wall (SWCNT) or multiwall carbon nanotubes (MWCNT) A SWCNT is a single graphene sheet rolled into a cylinder. A MWCNT consists of several coaxially arranged graphene sheets rolled into a cylinder. The graphene sheets are stacked parallel to the growth axis of carbon nanotubes, and their spacing was typically 0.34 nm [136]. Stacked-cup carbon nanotubes (SCCNTs) consisting of truncated conical graphene layers represent a new type of nanotubes. Multiwalled nanotubes may exhibit high degree of uniformity of internal diameter of single tubes, but with broad pore-size distribution in the micropore and mesopore ranges [137]. Typical characteristics of CNTs for use as catalyst support are an outer diameter of 10–50 nm, inside diameter of 3–15 nm, and length from 10 to 50 μm. As reported by Serp et al. [138], pores in MWNT can be mainly divided into inner hollow cavities of small diameter (narrowly distributed, mainly 3–6 nm) and aggregated pores (widely distributed, 20–40 nm) formed by interaction of isolated MWNT. On as-prepared and acid-treated SWNT, instead, adsorption of N_2 has clearly evidenced the microporous nature of SWNT samples [139]. Typically, total surface area of as-grown SWNT ranged between 400 and 900 $m^2 g^{-1}$, whereas, for as-produced MWNT values ranging between 200 and 400 $m^2 g^{-1}$ are often reported.

According to theoretical predictions, SWCNTs can be either metallic or semiconducting depending on the tube diameter and helicity [140]. For MWCNTs, scanning tunneling spectroscopy

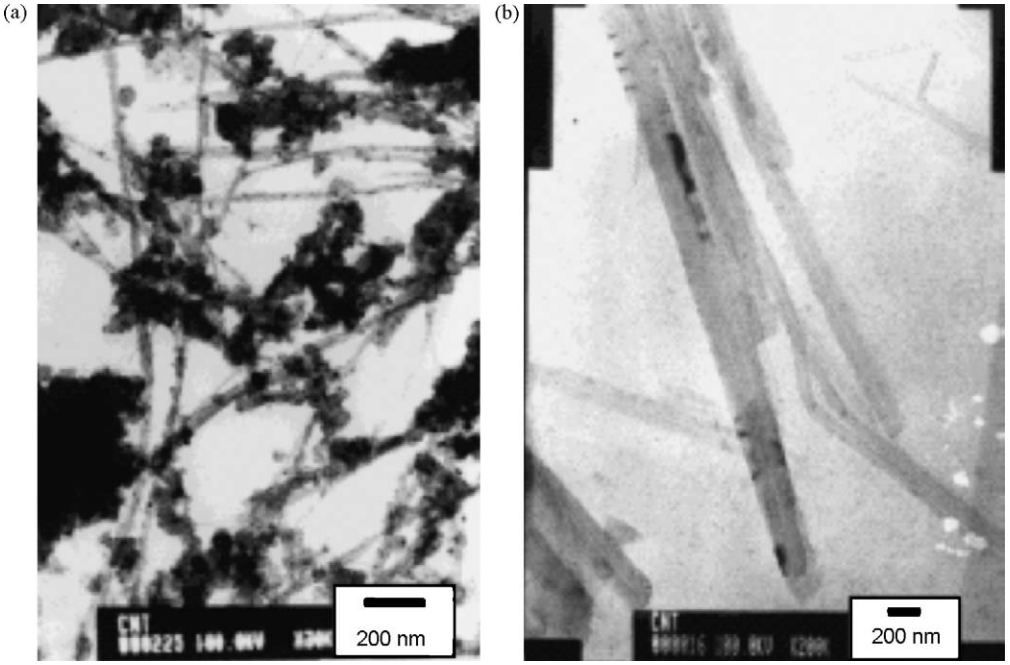

Fig. 8. Bright-field TEM micrographs of (a) MWNTs without purification and (b) MWNTs after purification and HNO_3–H_2SO_4 oxidation. Reproduced from Ref. [148], copyright 2003, from the American Chemical Society.

(STS) measurements indicate that the conduction is mainly due to the outer shell [141], which is usually much larger than SWCNTs. Therefore, MWCNTs should have a relatively high electrical conductivity. An important aspect of the MWCNTs is the high surface area for subsequent metal deposition. MWCNTs with small tube diameters (therefore high surface area) can be obtained using small catalyst particles for the synthesis [134]. There are four main CNTs growth methods: arc discharge [142], laser ablation [143], chemical vapour deposition [144] and plasma enhanced chemical vapour deposition (PECVD) [145–147]. Li et al. [148] synthesized MWCNTs from high-purity graphite in a classical arc-discharge evaporation method. The MWNTs, mostly ranging from 4 to 60 nm in diameter, were hollow tubular structures with a highly graphite multilayer wall. Fig. 8a from Ref. [148] shows that MWNTs are stacked onto each other, accompanied by many carbon nanoparticles and many carbonaceous impurities. The MWNTs, after treatment by purification and slow oxidation in a mixture of HNO_3–H_2SO_4, are shown in Fig. 8b, from which it can be seen that most MWNTs are isolated and nearly no carbon nanoparticle agglomeration is observed. In CVD, CNTs are grown using the catalytic decomposition of hydrocarbons over transition metal catalysts such as iron, cobalt and nickel at temperatures ranging from 550 to 1000 °C [143]. Much lower growth temperatures can be reached when PECVD is used [147], opening the possibility to use temperature sensitive substrates like plastics [149].

3.2.2. Metal dispersion: functionalized CNTs

Wildgoose et al. [150] reviewed the recent developments in CNT-supported catalysts by exploring the various techniques to load the carbon nanotubes with metals and other nanoparticles and the diverse applications of the resulting materials. More specifically, Lee et al. [151] reviewed the synthesis of carbon nanotube- and nanofiber-supported Pt electrocatalysts for PEM fuel cell, especially focusing on cathode nano-electrocatalyst preparation methods. Without surface modifications, however, most of CNTs lack sufficient binding sites for anchoring precursor metal ions or metal nanoparticles, which usually lead to poor dispersion and aggregation of metal nanoparticles, especially at high loading conditions. Indeed, while highly dispersed high loading metal nanoparticles have been obtained on carbon blacks, only less than 30 wt% Pt/MWCNT catalysts can be achieved because high Pt loading on unfunctionalized carbon nanotubes tend to aggregate [132,152,153]. Therefore, functionalization of CNTs is generally prerequisite to further applications. Analogously to carbon blacks, to introduce more binding sites and surface anchoring groups, an acid oxidation process was very frequently adopted by treating CNTs in a refluxed, mixed acid aqueous solution, commonly H_2SO_4/HNO_3 solution, at temperatures in the range 90–140 °C [133,154–156]. This treatment introduces surface-bound polar hydroxyl and carboxylic acid groups for subsequent anchoring and reductive conversion of precursor

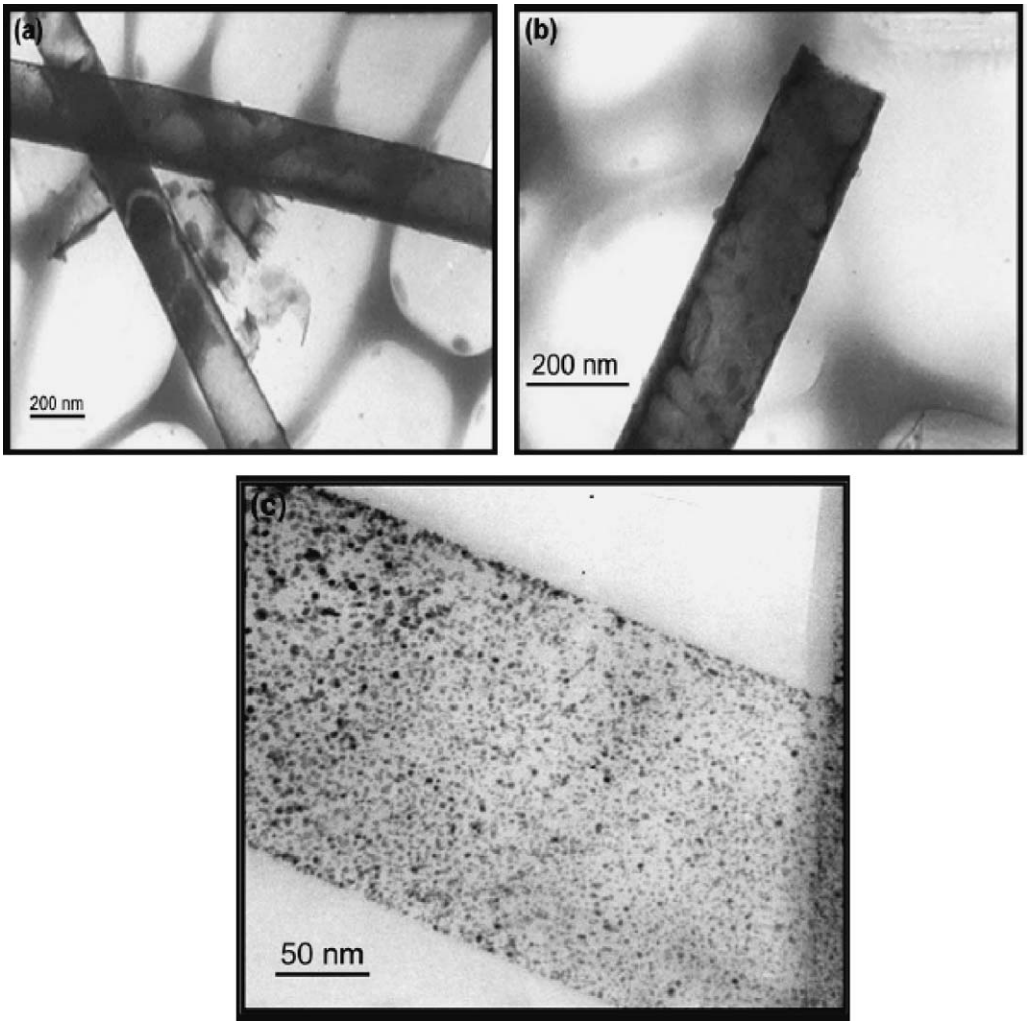

Fig. 9. TEM images of the nitrogen containing carbon nanotubes: (a) at lower magnification; (b) at higher magnification image of the individual nanotube (an arrow indicating the open end of the tube) and (c) Pt filled nitrogen containing carbon nanotubes. Reproduced from Ref. [51], copyright 2005, with permission from Elsevier.

metal ions to metal nanoparticles. Xing [133] used a sonochemical technique to oxidize the walls of the nanotubes while breaking bonds and leaving behind negatively charged functional groups. Prabhuram et al. [154] compared the particle size of PtRu catalysts supported on a functionalized MWCNT with that of PtRu supported on as-received Vulcan XC-72, both the catalysts prepared by the impregnation method using $NaBH_4$ as the reducing agent, and having a metal loading of 20 wt%. The resulting PtRu particle size was independent of the type of support. In the same way, Zhang et al. [155] compared metal dispersion of functionalized MWCNT and as-received Vulcan XC-72-supported Pt with metal loading of 40 wt% prepared by a chemical reduction method. Pt nanoparticles were homogeneously dispersed on the MWCNT and Vulcan XC-72. Average size of Pt particle on MWCNT and Vulcan XC-72 were 3.5 and 3.0 nm, respectively. Recently, Poh et al. [42] found that citric acid treatment of CNTs produces more functional groups such as carboxyl and hydroxide on the carbon surface than HNO_3–H_2SO_4 treatment.

The functionalization of CNT surface can occur not only before but also together with metal deposition on the carbon. Saha et al. [157] synthesized Pt nanoparticles supported on multiwalled carbon nanotubes grown directly on carbon paper by a new method using glacial acetic acid as a reducing agent. The glacial acetic acid acts as a reducing agent and has the capability of producing a high density of oxygen-containing functional groups on the surface of CNTs that leads to high density and monodispersion of Pt nanoparticles. Ag, Pd and PtRu nanoparticles were dispersed on SWCNT by Oh et al. [158] using gamma irradiation at room temperature. The attachment of the nanoparticles onto SWCNT was strong enough to be present even after chemical cleaning and ultra-sonication. FT-IR spectroscopy gave evidence for the surface modification of SWCNTs through the presence of characteristics peaks of carboxyl and hydroxyl groups.

Pyrolysis of nitrogen containing polymers is a facile method for the preparation of carbon nanotube materials containing nitrogen substitution in the carbon framework. Nitrogen containing carbon nanotubes (N-CNT) were synthesized by impregnating polyvinylpyrrolidone inside the alumina membrane template and subsequent carbonization of the polymer [50]. Maiyalagan et al. [51] prepared nitrogen-containing CNT, containing about 87.2 wt% carbon and 6.6 wt% nitrogen. Platinum nanoclusters were loaded inside the N-CNT by impregnation of the C/alumina composite with H_2PtCl_6. Then, Pt ions were reduced to Pt^0 by flowing H_2 at 550 °C. Finally, the underlying alumina was dissolved by immersing the composite in 48% HF for 24 h. TEM images of N-CNTs and Pt/N-CNT are shown in Fig. 9. The open end of the tubes observed by TEM showed that the nanotubes are hollow and the outer diameter of the nanotube closely match with the pore diameter of template used, with a diameter of 200 nm and a length of approximately 40–50 μm. Fig. 9c shows the TEM image of N-CNT-supported Pt nanoparticles. TEM pictures reveal that the Pt particles have been homogeneously dispersed on the nanotubes and particle sizes were found to be around 3 nm. According to the authors, nitrogen containing carbon nanotubes obtained in their study contains heterocyclic nitrogen so that it preferentially attaches the Pt particles.

As in the case of carbon blacks [48,49], also CNTs were functionalized with sulfonic acid [159–163]. Hudson et al. [159,160] reported the functionalization of CNTs using sodium nitrite to produce intermediate diazonium salts from substituted anilines, forming benzenesulfonic group on the surface of CNTs, which improve the solubility in water. Yang et al. [161] loaded palladium particles on the MWCNTs, which were functionalized in a mixture of 96% sulfuric acid and 4-aminobenzenesulfonic acid (f-MWCNT). Fig. 10 shows the HRTEM images of the Pd/MWCNTs (Fig. 10a) and Pd/f-MWCNTs (Fig. 10b) catalysts. Pd dispersion on unsulfonated MWCNTs is low and large Pd clusters can be seen in Fig. 10a. In Fig. 10b, instead, a higher Pd dispersion can be observed on f-MWCNTs. Although agglomeration of Pd nanoparticles still exists, it can be seen from this image that the dispersion of Pd nanoparticles on f-MWCNTs is greatly improved. According to the authors, it is due to the chemically active and hydrophilic surface of MWCNTs after benzenesulfonic functionalization. It has to be remarked that the f-MWCNTs supported Pd particles were synthesized completely in an aqueous phase by using $NaBH_4$ as a reducing agent. Being the f-MWCNTs more soluble in water than MWCNT, it is more simple to load the nanoparticles on the f-MWCNTs substrate. Du et al. [162] grafted sulfonic acid groups onto the surface of carbon nanotube-supported platinum (Pt/CNT) catalysts by both thermal decomposition of ammonium sulfate and in situ radical polymerization of 4-styrenesulfonate. The PEFC electrodes with the Pt/CNT catalysts sulfonated by the in situ radical polymerization of 4-styrenesulfonate exhibited better performance than those with the unsulfonated counterparts, mainly because of the easier access with protons and well dispersed distribution of the sulfonated Pt/CNT catalysts.

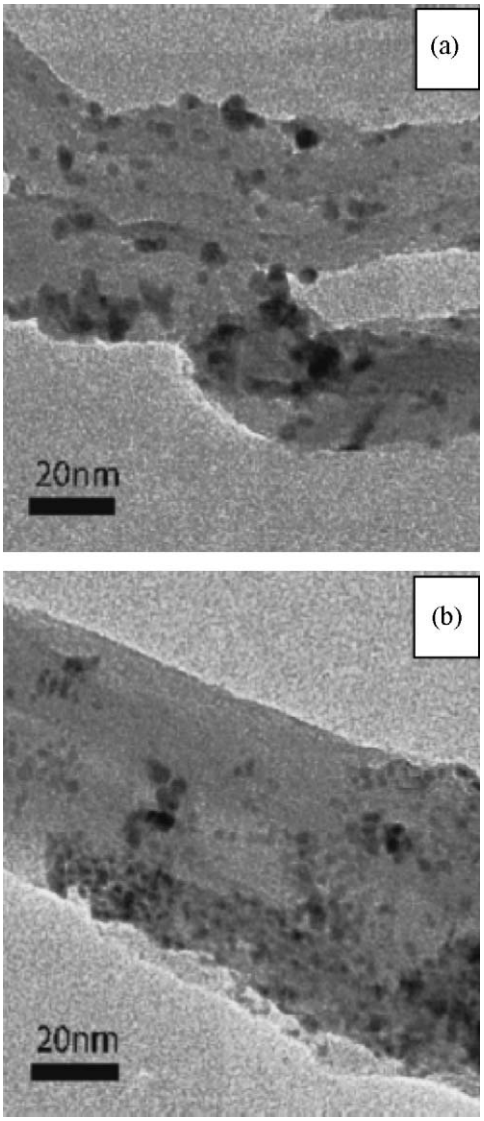

Fig. 10. HRTEM of Pd supported on unsulfonated (a) and sulfonated (b) MWCNTs. Reproduced from Ref. [161], copyright 2008, with permission from Elsevier.

3.2.3. Electrochemical properties

Regarding the electrochemical activity of CNT-supported catalysts it has to be prudent. Most papers are indeed very optimistic regarding the potential interest of CNT, due to presumable high activity of CNT-supported metals. In some cases the authors overvalue their results, for example comparing CNT-supported catalysts with bad CB supported catalysts. As reported in a lot of papers [51,131,148,154–156,163–172], when used as anode and/or cathode materials in low-temperature fuel cells, Pt and Pt-M catalysts supported on carbon nanotubes presented higher catalytic activity than that of the same catalysts supported on carbon blacks. The higher activity of CNT-supported metal with respect to CB supported metal was ascribed to different factors:

(1) The crystalline nature of CNTs [59,129] allows carbon nanotubes act as a good conductive substrate: the higher conductivity of CNTs is considered to contribute to the high performance of the CNT-supported metal electrodes. It has to be remarked, however, that the functionalization of the CNTs lowers their conductivity, As reported by Bekyarova et al. [173], chemical functionalization of SWNTs with octadecylamine (ODA) and poly(*m*-aminobenzenesulfonic acid) (PABS) significantly decreases the conductivity from 250–400 S cm^{-1} to 3 and 0.3 S cm^{-1} for SWNT–ODA and SWNT–PABS, respectively.
(2) The hollow cavity and graphitic layer interspaces give more access to the gases than conventional supports. The Vulcan carbon support has randomly distributed pores of varying sizes which may make fuel and product diffusion difficult whereas the tubular three-dimensional morphology of the carbon nanotubes makes the fuel diffusion easier [51,155].
(3) The chemical differences between CNT and carbon black induce flat disposition for Pt on the surface of CNT. This configuration of the Pt crystallite leads to a decrease in the adsorption energy of hydrogen as deduced from temperature-programmed decomposition (TPD) measurements. Their contention is that the decrease in the adsorption energy can be due to lowering of the d band centre induced by the reduction of the Pt lattice constant. However, the alteration of the d band centre need not be only due to the variation in the lattice constant but also arise from the charge transfer from the anchoring sites of Pt. These changes in the electronic properties may be responsible for the improvement of the electrochemical reactions [163].
(4) The architecture of the carbon nanotubes can give rise to specific sites (edge sites) where the Pt crystallites are anchored and these sites may be more active than the conventional sites obtainable in carbon blacks. Essentially carbon blacks normally present equi-potential sites, and hence almost all Pt sites will be equally moderately active. The tubular morphology of carbon nanotubes, instead, can provide specific active sites for anchoring Pt crystallites and hence the activity of the resulting system can be different from what is obtainable in conventional carbon black supports [174].
(5) A low degree of alloying for MWCNT-supported PtRu with respect to PtRu supported on CB [154]. Indeed, as reported by Long et al. [175], non-alloyed PtRu seems to more electrocatalytically active than high alloyed PtRu.
(6) The presence of different Pt crystallite phases on the MWCNTs and on the carbon, it is believed from these findings that the existence of the distinctive Pt crystallite phases, i.e. Pt(1 1 0), on the PtRu particles supported on the MWCNTs could be reason for enhancing the activity of the methanol oxidation reaction [154].

Maiyalagan et al. [51] reported that the nitrogen containing carbon nanotube-supported Pt shows a ten-fold increase in the catalytic activity compared to the commercial Vulcan supported Pt. The higher electrocatalytic activity of Pt/N-CNT was ascribed to the higher dispersion and a good interaction between the support and the Pt particles. According to the authors, the nitrogen functional group on the carbon nanotubes surface intensifies the electron withdrawing effect against Pt and the decreased electron density of platinum facilitate oxidation of methanol. However there is an optimum amount of nitrogen content necessary for increased activity for methanol oxidation. This optimum amount is around 10% which shows that the isolated nitrogen sites favour the better dispersion of Pt and also controls the metal crystallite sizes [176]. According to Du et al. [177], the N-dopants in CNT serve as the defect sites to enhance nucleation of Pt particles.

Wu and Xu [178] presented a detailed comparison between multiwalled and single-walled carbon nanotubes in an effort to understand which can be the better candidate of a future supporting carbon material for electrocatalyst in direct methanol fuel cells. Pt particles were electrodeposited on MWCNT/Nafion and SWCNT/Nafion electrodes to investigate effects of the carbon materials on the physical and electrochemical properties of Pt catalyst. CO stripping voltammograms showed that the onset and peak potentials on Pt-SWCNT/Nafion were significantly lower that those on the Pt-MWCNT/Nafion catalyst, revealing a higher tolerance to CO poisoning of Pt in Pt-SWCNT/Nafion. In the methanol electrooxidation reaction, Pt-SWCNT/Nafion catalyst was characterized by a significantly higher current density, lower onset potentials and lower charge transfer resistances. Therefore, SWCNT presents many advantages over MWCNT and would emerge as an interesting supporting carbon material for fuel cell electrocatalysts. The enhanced electrocatalytic properties were discussed based on the higher utilization and activation of Pt metal on SWCNT/Nafion electrode. The remarkable benefits from SWCNT were further explained by its higher electrochemically accessible area and easier charge transfer at the electrode/electrolyte interface due to SWCNT's sound graphitic crystallinity, richness in oxygen-containing surface functional groups and highly mesoporous 3D structure. Carmo et al. [134] tested the catalytic activity of PtRu supported on SWCNT, MWCNT and Vulcan XC-72R carbons as anode material in DMFC. Conversely to the results of Wu and Xu [178], the MOR activity was in the order PtRu/MWCNT > PtRu/C > PtRu/SWCNT.

Also cup-stacked-type carbon nanotubes have been investigated as a catalyst support for the direct methanol fuel cells by the electrochemical oxidation of methanol at various temperatures [131]. The CSCNT-supported PtRu catalyst exhibited twice as high a power density as the PtRu catalyst supported on Vulcan XC-72 carbon. The microscopic analysis of the CSCNT-supported Pt-Ru catalysts revealed that the bimetallic electrocatalysts were well dispersed on the CSCNT supports, and the particle size of the electrocatalysts was ca.5 nm.

3.2.4. Stability of CNT-supported catalysts

Long-term stability of supported catalysts is an important parameter for practical applications. Maiyalagan et al. [51] investigated the durability of various electrodes by chronoamperometry measurements in H_2SO_4/CH_3OH at 0.6 V. The nitrogen containing carbon nanotube electrodes were the most stable for direct methanol oxidation. The increasing order of stability of various electrodes was; Pt < Pt/Vulcan < Pt/N-CNT. According to the authors, the tubular morphology and the nitrogen functionality of the support have influence on the dispersion as well as the stability of the electrode.

Wang et al. [179] showed that multiwalled CNTs can be more durable and can outlast the lifetime of conventional Vulcan XC-72. Electrochemical surface oxidation of carbon black Vulcan XC-72 and multiwalled carbon nanotube has been compared following potentiostatic treatments up to 168 h under condition simulating PEMFC cathode environment (60 °C, N_2 purged 0.5 M H_2SO_4, and a constant potential of 0.9 V). The subsequent electrochemical characterization at different treatment time intervals suggests that MWCNT is electrochemically more stable than Vulcan XC-72 with less surface oxide formation and 30% lower corrosion current under the investigated condition. As a result of high corrosion resistance, MWCNT shows lower loss of Pt-surface area and oxygen reduction reaction activity when used as fuel cell catalyst support.

The long-term performance of PtRu particles supported on MWCNTs and on carbon black towards the methanol oxidation reaction was compared by Prabhuram et al. [154]. They carried out chronoamperometry tests in 0.5 M H_2SO_4 solution containing methanol for 3000 s. The close observation of the chronamperometry curves revealed that potentiostatic current decreases very rapidly for MWCNT-supported PtRu. According to the authors, this might be due to the higher deactivation of the Pt(1 1 0) crystallite phase by the CO_{ads} species during the methanol oxidation reaction. At long times, however, although the current gradually decays for all the catalysts, the MWCNT-supported PtRu catalysts maintained a slightly higher current than the carbon black supported PtRu.

Finally, Girishkumar and co-workers [171] found by accelerated durability tests carried out in $HClO_4$ solution using Pt/SWCNT and Pt/C films cast on a rotating disk electrode that SWCNTs enhance the stability of the electrocatalyst during long-term use. Although Pt/C has a higher electrochemically active surface area than Pt/SWCNT before the durability test, the ECSA of Pt/C decreased continuously with potential cycling, and finally decreased below ECSA of Pt/SWCNT after 36 h of potential cycling. Pt/C lost 50%, whereas Pt/SWCNT lost only 16% of ECSA. These results indicate a lower degree of recrystallization of Pt particles on SWCNT and a greater stability of SWCNT to anchor Pt particles. According to the authors, these accelerated stability tests suggests that SWCNT is a superior support to anchor Pt particles. In addition to the improved catalytic activity, the SWCNT support minimizes the Pt aggregation effect during long-term usage.

Summarizing, the results regarding the CNT stability are very promising, but they are scarce and carried out in acidic solution. Further tests, particularly in a single fuel cell, have to be performed to confirm the good long-term performance of the CNTs as a support for fuel cell catalysts.

3.3. Carbon nanohorns and nanocoils

Carbon nanohorns and carbon nanocoils, as well as carbon nanotubes, constitute a new class of carbon nanomaterials with properties that differ significantly from other forms of carbon. These materials have been tested as support for fuel cell metal catalysts. The high catalytic activity of carbon nanohorn/carbon nanocoil supported catalysts demonstrates the suitability of their application in fuel cell technology.

Single-wall carbon nanohorn (SWCNH) aggregates can be produced by CO_2 laser vaporization of carbon, and a single aggregate can take either a "dahlia-like" or "bud-like" form. Kasuya et al. [180] found that "dahlia-like" SWCNH aggregates were produced with a yield of 95% when Ar was used as the buffer gas, while "bud-like" SWCNH aggregates were formed with a yield of 70 or 80% when either He or N_2 was used. Yudakasa et al. [181] obtained single-wall carbon nanohorns, 30–50 nm long and 2–3 nm thick, forming aggregates that resemble dahlia flowers (diameter: 80 nm). CO_2 laser vaporization of graphite at room temperature produced a high yield (about 75%) of SWCNHs.

The structure of a nanocoil is similar to that of MWCNTs, except helical shape. It can be therefore said that a carbon nanocoil is a helical MWCNT [182,183]. Choi et al. [182] grew carbon nanocoils on quartz substrates onto which indium tin oxide (ITO) thin film had been formed. The elemental ratio of Sn/(In + Sn) in sputtering target was 50%. Then, Fe-containing solution was spread on ITO film by spin coating with two different spinning rates of 500 rpm and 1000 rpm. Carbon nanocoils were grown at 700 °C for 30 min using C_2H_4 gas.

Few works have been performed on catalysts supported on CNHs or CNCs for use in low-temperature fuel cells. For this reason, at this time, notwithstanding the encouraging results, it is hazardous to affirm that the electrochemical activity of CNH and CNC supported catalysts is higher than that of CB supported catalysts. Sano and Ukita [184] synthesized SWCNH supported Pt by arc plasma in liquid nitrogen using Pt-contained graphite anode. The size distribution of Pt particles can be controlled by adjusting the concentration of Pt in the graphite anode. Approximately 90% among the Pt particles had a particle size lower than 5 nm. They verified that the as-grown Pt-loaded products produced by this method can be useful for the use in polymer electrolyte fuel cell. Yoshitake et al. [185] prepared a platinum catalyst supported on single-wall carbon nanohorn. The Pt particles were homogeneously dispersed on the SWCNH, and their particle size was about 2 nm. This size was less than half of that supported on conventional carbon black. A fuel cell using the SWCNH showed a larger current density than one using the carbon black.

Park and co-workers [64,186] employed carbon nanocoils with variable surface areas and crystallinity as the supports for 60 wt% Pt/Ru catalysts. The catalysts supported on all the carbon nanocoils exhibited better electrocatalytic performance compared to the catalyst supported on Vulcan XC-72 carbon. In particular, the PtRu alloy catalyst supported on the CNC, which has both good crystallinity and a large surface area, showed a superior electrocatalytic performance, compared to the other CNC catalysts. Sevilla et al. [187] synthesized highly graphitic carbon nanocoils by the catalytic graphitization of carbon spherules obtained by the hydrothermal treatment of different saccharides (sucrose, glucose and starch). These carbon nanocoils were used as a support for PtRu nanoparticles, which were well dispersed over the carbon surface. They tested PtRu/CNC as an electrocatalyst for methanol electrooxidation in an acid medium, and found that the carbon nanocoil supported PtRu nanoparticles exhibit a high catalytic activity, which is even higher than that of PtRu supported on Vulcan XC-72R. They ascribed the high electrocatalytic activity of the PtRu/CNC catalyst to the combination of a good electrical conductivity, derived from their graphitic structure, and a wide porosity that allows the diffusional resistances of reactants/products to be minimized.

3.4. Activated carbon fibers (ACFs) and carbon/graphite nanofibers

It is well known that fibers offer flexibility which does not apply to the usual powdery or granular materials. Fibrous catalytic packs offer the advantages of an immobile catalyst and a short diffusion distance. Another advantage of fibrous catalysts is their low resistance to flow of liquid and gases through a bundle of fibers. Thus, they can be used as an attractive alternative in fuel cell.

To use as catalyst support carbon fibers can be activate by carbonizing at high temperature or treated to form carbon (graphite) nanofibers.

3.4.1. Activated carbon fibers

Activated carbon fibers represent a novel kind of porous material, with high surface area (>1000 $m^2\ g^{-1}$), and the presence of a lot of functional groups on the surface [188]. Bulushev et al. [189] characterized activated carbon fibers in the form of a woven fabric by temperature-programmed decomposition. TPD method showed the presence of two main types of functional groups on the ACF surface: the first type was associated with carboxylic groups easily decomposing to CO_2, and the second one corresponded to more stable phenolic groups decomposing to CO. Parmentier et al. [188] prepared ACFs by carbonizing a rayon fabric. The carbonization of the rayon fabric includes a pre-carbonization stage performed at a temperature in the range 350–420 °C, and the activation, performed at a temperature in the range 850–950 °C. under CO_2. Activate rayon-precursor carbon fibers can present pores with a mean size in the range 0.3–3 nm for filaments with a diameter in the range 5–20 μm, and with a total porosity of 30–50% by volume. This favours great dispersion of the catalyst in the form of fine particles of a size not exceeding 3 nm. Another advantage of activate rayon-precursor carbon fibers consists in the high purity of the resulting carbon fibers: a carbon content greater than 99%, an ash content less than 0.3%, and an alkaline impurity content of less than 1500 ppm. Thus, acid washing treatment prior to catalyst fixing is not necessary. In addition, fibers make it possible to form substrates that are particularly suitable for receiving metal catalysts such as platinum and ruthenium. Furthermore, carbon derived from a rayon precursor is hydrophilic and consequently favours exchange with liquids, in particular aqueous media. Huang et al. [190] prepared ACFs using viscose fibers, carbonized at 850 °C in N_2 atmosphere and activated using steam as an activation agent at the same temperature for 60 min. Viscose-based activated carbon fiber thus obtained had diameters of about 10 μm.

ACF has such a reduction property that it can reduce Pt(IV) and Pd(II) into metallic elements [168,191], which leads to a promising application of being used in the preparation of catalysts without necessarily requiring special surface oxidation as is usually the case with CB and CNT. de Miguel et al. [192] prepared ACF supported Pt by the impregnation method using chloroplatinic acid as metal precursor. They investigated the effect of impregnation time and surface chemistry of the support on the catalytic properties and the characteristics of the metallic phase. The state of platinum in reduced catalysts (at 100 and 350 °C) was studied by TPR and XPS. The use of low impregnation times (30 min) during the preparation of Pt/ACF leads to catalysts with Pt mainly deposited in the outer shell of the fibers, while at higher impregnation times, the metallic atoms seem to be deposited inside the pores. Pt(0) species appear in catalysts reduced at 100 °C by effect of the reducing properties of the carbon fiber.

ACF were tested as support for fuel cell catalysts. Zheng et al. [169] compared the catalytic activity for ethanol oxidation of Pd supported on MWCNT, CB and ACF prepared by the intermittent microwave heating technique. The order of ethanol oxidation activity was Pd/MWCNT > Pd/C > Pd/ACF. Huang et al. [190] prepared ACF supported Pt nanoparticles for use in direct alcohol fuel cells by polyol synthesis. HRTEM images of Pt/C and Pt/ACF catalysts are shown in Fig. 11. The image (see Fig. 11a) revealed that the Pt crystallites dispersed on ACF had relatively good crystallographic orientation, suggesting the establishment of a strong metal–support interaction. It might be due to the strong interactions between Pt particles and ACF, which are caused by the abundant functional groups such as carboxyl, hydroxyl and carbonyl groups on the surface of supports.

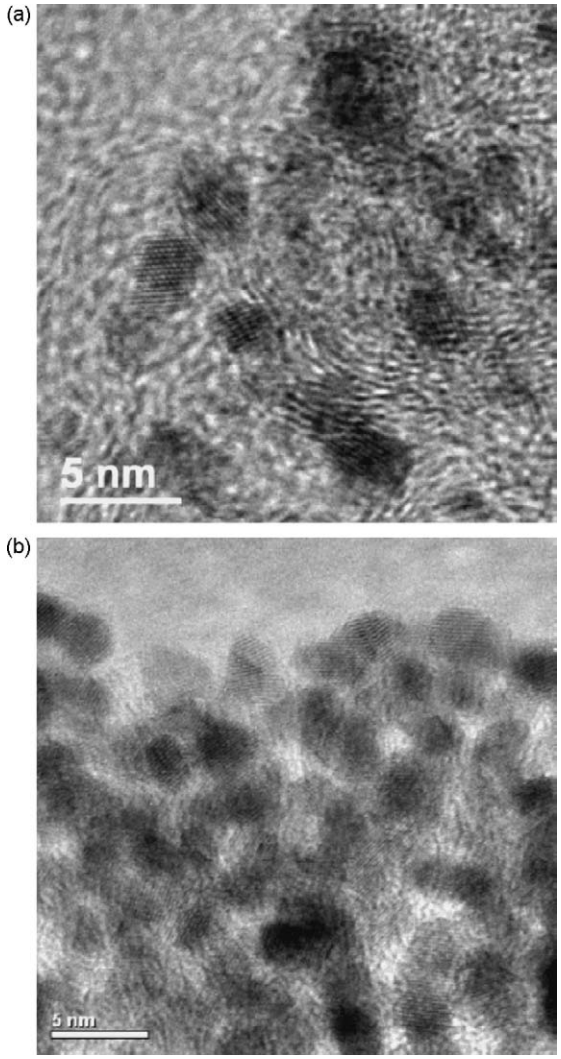

Fig. 11. HRTEM images of Pt/C (a) and Pt/ACF (b) catalysts. Reproduced from Ref. [190], copyright 2008, with permission from Elsevier.

Meanwhile, surface basic sites of ACF are associated with π-electron rich regions within the basal planes, which is also responsible for the strong adsorption of Pt. In contrast, Pt particles supported on Vulcan XC-72 were found to adopt a more dense globular morphology (see Fig. 11b), suggesting that in this case there was a relatively weak interaction with the metal and support. The mean size was estimated to be 2.4 nm for Pt/ACF and 2.9 nm for Pt/C. They investigated the oxidation of methanol, ethanol and isopropanol on Pt/C and Pt/ACF electrodes. The peak current densities for alcohol oxidation on Pt/ACF electrode were almost twice as that on Pt/C electrode; furthermore, the onset potentials for Pt/ACF electrocatalyst shifted to lower values compared with Pt/C electrocatalyst. Moreover, Pt/ACF presented higher stability than Pt/C. Indeed, the retention value of active surface area of Pt/ACF catalyst was gradually decreased with repetitious cycles to show the minimum value of 85.4% at around 1000 cycles. This value tended to keep constant afterwards, whereas the value for the Pt/C catalyst continued to drastically decrease down to 45% at 1800 cycles. According to the authors the improvement in the performance of Pt/ACF with respect to Pt/Vulcan was attributed both to the uniform dispersion of Pt nanoparticles and to the strong interactions between Pt nanoparticles and ACFs.

3.4.2. Carbon nanofibers

Carbon nanofibers are also named graphite nanofibers, and denoted as GNFs. In this review, we will use the notation CNF. Catalytically grown carbon nanofibers are novel materials that are the product of the decomposition of carbon-containing gases over certain metal surfaces [193]. CNFs have generated intense interest in terms of its application as a catalyst support material because of its unique structure [60,194–197]. There are various types of CNFs: platelet, ribbon, herringbone and spiral structures. The schematic representations of the "platelet", "ribbon", and "herring-bone" structures of CNFs are reported in Fig. 12 from Ref. [60]. Unlike conventional graphite materials and nanotubes where the basal plane is exposed, in the structure of CNF, only the edge regions are exposed [60]. The main difference between nanotubes and nanofibers consists in the lack of a hollow cavity for the latter. Due to their peculiar structure, CNFs are mainly used as catalytic supports without any pre-treatment: indeed platelets and herringbone structures present potentially reactive groups for metal anchoring. Several research groups synthesized carbon nanofibers on the surface of carbon fibers, using thermal CVD at temperatures between 600 and 660 °C. Downs and Baker [198,199] grew CNFs on the surface of carbon fibers in an ethylene-hydrogen environment using a copper-nickel (3:7) catalyst at 600 °C. The growth of carbon nanofilaments on the surface of carbon fibers improved the composite shear strength of the fibre by over 4.75 times, by forming interlocking networks and by increasing the surface area from 1 up to 300 $m^2\ g^{-1}$ [198]. Carbon nanofibers are grown by Boskovic et al. [200] on a carbon fiber cloth using plasma enhanced chemical vapour deposition from a gas mixture of acetylene and ammonia. A cobalt colloid is used as a catalyst to achieve a good coverage of nanofibers on the surface of the carbon fibres in the cloth. These CNFs, grown by a tip growth mechanism, showed a bamboo-like structure, reflecting higher degree of crystallinity, of the graphene layers with a characteristic interlayer spacing of 0.34 nm. Nanofibers grown on the surface of the carbon fibres present a preferential orientation in the direction of the applied electric field. The CNFs grown on the side facing the anode are straight and aligned towards the anode whereas the CNFs grown on the opposite side of the fiber are entangled. The length of these CNFs was between 1 and 5 μm with diameters in the range 10–80 nm. A similar wide diameter distribution was also found by Boskovic et al. [201] for CNF synthesis using Ni powder catalyst at substrate held at room temperature. Park et al. [194,195] obtained three types of CNFs by chemical vapour deposition method, i.e. ribbon-like, spiral-like and platelet-like. The surface areas of these CNFs were 85, 45 and 120 $m^2\ g^{-1}$, respectively. The diameter and length of the GNF were 100–150 nm and 5–50 μm, respectively. Carbon nanofibers were grown by Gangeri et al. [202] by chemical vapour deposition on two different types of micro-shaped carbon fibers supports (felt and cloth). The structure of CNFs was studied by TEM and some images are reported in Fig. 13. Low magnification image confirmed the lack of an hollow cavity in some parts and evidenced that no residual metallic particles, coming from the CNFs production process, could be observed because they were encapsulated by the carbon. In the high magnification TEM image, it was evident that carbon nanofibers were herringbone, that means graphene layers are stacked obliquely (75°) with respect to the growth axis and regularly spaced by a distance of about 0.34 nm.

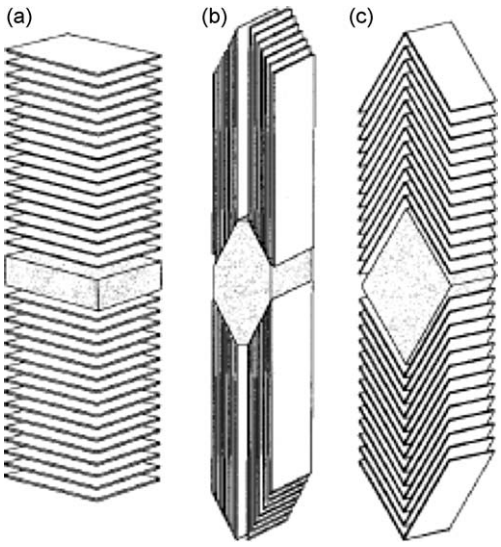

Fig. 12. The schematic representations of the "platelet", "ribbon", and "herring-bone" structures of GNF. Reproduced from Ref. [60], copyright 2001, from the American Chemical Society.

CNF-supported catalysts were prepared for use in fuel cells and their metal dispersion and catalytic activity was compared with that of other carbon supports [142,201–204]. Gangeri et al. [202] deposited Pt by incipient wetness impregnation on CNFs. Tests in PEMFC indicated that the cells with Pt/CNF as anode material better performed than those with Pt/Vulcan. Yuan and Ryu [203] showed that CNFs were able to give better performance as a catalyst support material for a polymer electrolyte membrane fuel cell compared to CNTs. Steigerwalt et al. [196] and Bessel et al. [60] demonstrated that CNF-supported catalysts showed improved activities for methanol oxidation. Bessel et al. [60] found that catalysts consisting of 5 wt% Pt supported on "platelet" and "ribbon" type graphite nanofibers, which expose mainly edge sites to the reactants, exhibit activities comparable to that displayed by about 25 wt% Pt on Vulcan carbon. Furthermore, they observed that the graphite nanofiber-supported metal particles were significantly less susceptible to CO poisoning than the traditional catalyst systems. According to the authors, this improvement in performance is believed to depend on the fact that the metal particles adopt specific crystallographic orientations when dispersed on the highly tailored graphite nanofiber structures. Park et al. [197] prepared CNF-supported PtRu catalysts by the borohydride reduction method. Generally, it is difficult to obtain high-loaded and well dispersed PtRu metal catalysts on CNFs by conventional methods. However, they obtained highly dispersed PtRu particles on CNF and the herring-bone structure of CNF, as shown in Fig. 14. The images shown in Fig. 14b indicate that the dispersed crystallites on CNFs have relatively faced and highly ordered structures. Although CNFs have a small surface area for metal loading, the catalytic activities of CNF-supported PtRu nanoparticles were higher than those of Vulcan XC-72-supported catalyst. The electrochemical measurements indicated that the CNF-supported catalyst has a similar value in the mass-normalized currents and an increased value in the area-normalized currents, compared to the Vulcan XC-72-supported catalyst. According to the authors, this indicates that the enhancement in catalytic activity of the CNF-supported catalyst is the result of interactions between metal particles and CNFs. In particular, CNFs might modify the geometric characteristic of the supported catalysts.

Knupp et al. [130] investigated the electrochemically active surface area of Pt supported on CNT, CNF and CB They found that the CB supported catalyst has an ECSA of 50 $m^2\ g^{-1}$, which is lower than that of both the CNT and CNF-supported catalysts. In addition, CNF-supported catalyst gave comparable ECSA as the more expensive CNT, making it a more attractive candidate for future works in this area.

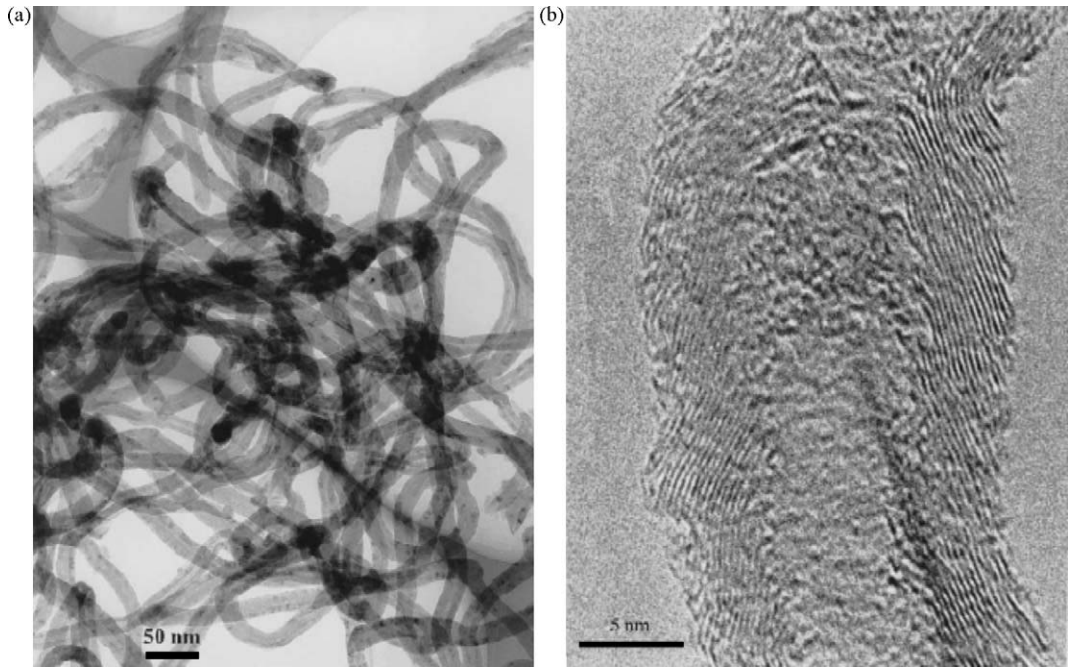

Fig. 13. TEM images of CNFs at low (a) and high (b) magnification. Reproduced from Ref. [202], copyright 2005, with permission from Elsevier.

3.5. Boron-doped diamonds (BDDs)

Polycrystalline boron-doped diamond possesses properties ideally suited for an electrocatalyst support for fuel cells. The material possesses superior morphological stability and corrosion resistance, compared to conventional sp^2 carbon support materials, being able to withstand current densities on the order of 1 A cm^{-2} for days, in both acidic and alkaline conditions, without any evidence of structural degradation [205,206]. The material is chemically inert allowing for its use at elevated temperatures in oxidizing or reducing media without loss of properties. The electrically conductivity of diamond remarkably increases after boron doping. BDD powder was prepared by Fischer and Swain [207] by coating insulating diamond powder (8–12 μm diameter, ~2 m^2 g^{-1}) with a thin boron-doped layer using microwave plasma-assisted chemical vapour deposition. As shown in Fig. 15 from Ref. [207], scanning electron microscopy revealed that the diamond powder particle edges become smoother and more well-defined faceting develops. Many of the particle surfaces consist of multiple grooves along the edges of the triangular facets. Fusion of neighboring particles was also observed with increasing growth time. Electrical resistance measurements of the bulk powder (no binder) confirmed that a conductive diamond overlayer formed, as the conductivity increased from near zero (insulating, $<10^{-5}$ S cm^{-1}) for the uncoated powder to 1.5 S cm^{-1} 1 after the 6-h growth.

Regarding the formation of diamond supported catalysts, firstly, Awada et al. [208] demonstrated that some metals such as Pt, Pb and Hg can be electrochemically deposited on the surface of conductive diamond thin films. Bennett et al. [209] reported the pulsed galvanostatic deposition of nanometer-sized Pt particles on electrically conducting microcrystalline and nanocrystalline diamond thin-film electrodes. The deposition was studied as a function of pulse number (10–50) and current density (0.50–1.50 mA cm^{-2}) at the two morphologically different forms of diamond. The deposition of catalyst particles using ten pulses at a

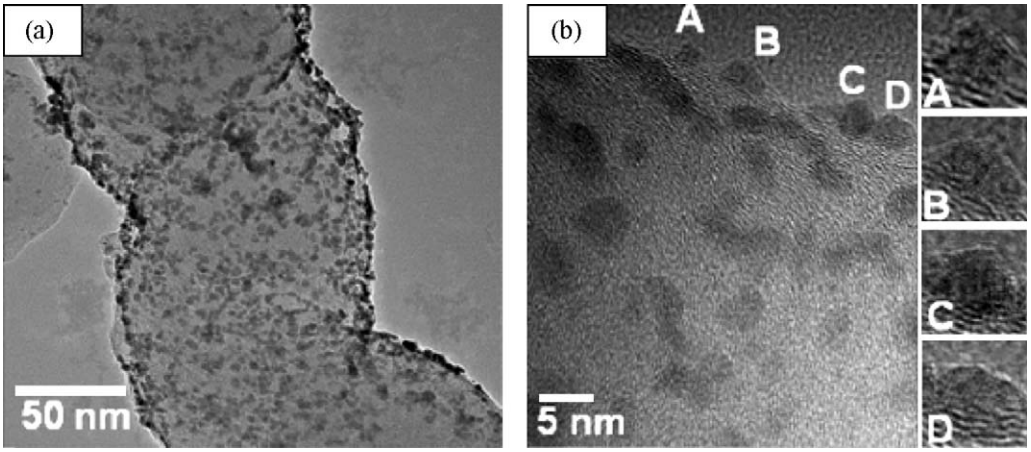

Fig. 14. Field emission transmission electron microscopy (FETEM) images of metal particles on the CNF. Low-resolution image (a) represents the dispersion of metal particles and high-resolution image (b) shows lattice patterns of metal particles on the edge of the GNF. Reproduced from Ref. [197], copyright 2007, with permission from Elsevier.

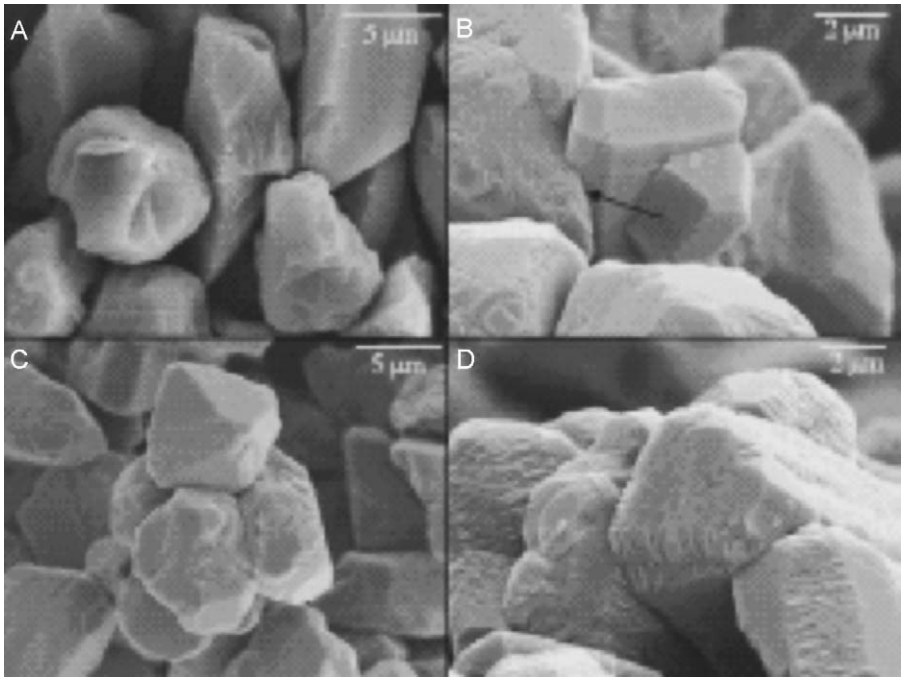

Fig. 15. SEM images of (a) bare diamond powder and conductive diamond powder at (b) 1 h, (c) 2 h, and (d) 4 h coating times. Reprinted from Ref. [207], copyright 2005, with permission from The Electrochemical Society.

current density of 1.25 mA cm^{-2} produced the smallest nominal particle size and the highest particle coverage on both diamond surfaces. SEM analysis revealed metal particle deposition over much of the diamond surface, a nominal particle size of 43 nm for microcrystalline and 25 nm for nanocrystalline diamond. Deposition under these conditions resulted in the most efficient utilization of the metal catalyst for H^+ adsorption, based on the electrochemically active Pt area normalized to the estimated metal loading. Typical specific surface areas of 10–50 $m^2\ g^{-1}$ Pt were calculated. On this basis, boron-doped diamond could be a possible alternative to carbon as a support material for fuel cell electrocatalysts. These catalysts, however, showed low long-term stability. Long-term potential cycling of BDD supported Pt between −400 and 1500 mV vs. Ag/AgCl in 0.1 M $HClO_4$ was performed for one thousand cycles at a potential scan rate of 0.05 V s^{-1} by Awada et al. [207]. The hydrogen desorption charge prior to cycling was 800 mC cm^{-2} and decreased significantly to 25 mC cm^{-2} after cycling, with a decrease of over 96%. Honda et al. [210] studied the electrocatalytic behavior of boron-doped nanoporous honeycomb diamond films modified with Pt nanoparticles using cyclic voltammetry and electrochemical impedance spectroscopy in acid solution. The current density in the CV for methanol oxidation at a Pt-modified BDD porous film with a pore diameter of 400 nm and a pore depth of 3 μm, was greatly enhanced, by a factor of 16, in comparison to the values obtained with a bulk Pt electrode. This enhancement was attributed to both the high surface area of the nano-honeycomb structure and the high electrocatalytic activity of Pt nanoparticles dispersed inside the pores. The electrocatalytic activities of the Pt-modified nano-honeycomb films were found to be dependent on the structural parameters of the honeycomb pores. Wang et al. [211] co-deposited a polycrystalline, boron-doped diamond thin film with Pt on a conducting Si (1 0 0) or Pt substrate. The resulting dimensionally stable and corrosion-resistant diamond thin film consisted of well-faceted microcrystallites with dispersed Pt particles incorporated into the surface. The metal particles were anchored into the diamond surface and range in diameter from 10 to 500 nm. The as-dispersed Pt particles were electroactive for the methanol oxidation. Montilla et al. [212] used two methods for the deposition of Pt particles on BDD surfaces: chemical deposition and electrodeposition under potentiostatic conditions. Electrodeposition lead much higher platinum dispersion than chemical deposition. The Pt modified BDD electrodes were tested for the oxidation of methanol, showing that multi-step deposition results in higher values of surface and mass activities for methanol oxidation than one-step deposition process. However, the stability of these materials was unsatisfactory and 65% of the Pt was removed from the surface after 1000 voltammetric cycles. Salazar-Banda et al. [213] investigated the modification of boron-doped diamond electrodes with platinum oxide particles deposited by the sol–gel method and using several pre- and post-treatments of the surface. The electrochemical stability of the resulting catalytic coatings in acid medium was much greater than those previously reported in the literature for others deposition methods. A thermal pre-treatment of the BDD surface yielded electrodes that retained 91.6% of the coated material after 1000 voltammetric cycles carried out between the water decomposition reactions. The application of a Nafion® film on top of the coating preserved integrally the deposited platinum oxide. These results clearly indicate that the sol–gel method produces more stable PtO_x deposits on BDD surfaces than other reported techniques even when only a cathodic surface pre-treatment is used. Moreover, the use of a thermal pre-treatment considerably increases the stability while covering the surface with a Nafion® film makes the clusters detachment/dissolution become negligible. The same research group [214,215] fixed Pt, Pt-RuO_2/C and Pt-RuO_2-RhO_2 on the surface of a boron-doped diamond (BDD) electrode by sol gel method. By cyclic voltammetry, Tafel plots and chronoamperometry measurements the ethanol oxidation in H_2SO_4 solutions on these BDD supported catalysts occurred with larger current densities and increased stability than that on a commercial Pt/C catalyst.

Siné et al. prepared bimetallic binary Pt-Sn [216] and ternary Pt-Ru-Sn [217] nanoparticles supported on a boron-doped diamond substrate. These nanoparticles showed high activity towards

methanol and/or ethanol oxidation. They believed that this substrate could promote the activation of the ethanol C–C bond scission, or increase the turnover frequency of product formation. The positive effect of Nafion as stabilizer agent was observed also by Spataru et al. [218]. They prepared a Pt/BDD powder electrocatalyst via electrochemical deposition of platinum, and compared the electrochemical behavior with that for Pt/graphite powder. The BDD deposited Pt particles were rather uniform in size (5–15 nm), although they form particle clusters. Electrodes were prepared by coating polycrystalline BDD films with these electrocatalysts, with Nafion solution as a binder, and the activities for methanol oxidation were found to be comparable. The use of BDD/Nafion resulted in a much higher stability of the catalyst under severe anodic conditions. Steady-state and long-time methanol oxidation polarization measurements, performed in the "floating electrode" configuration in acidic media, showed that platinum on BDD powder was less sensitive to deactivation, presumably due to CO poisoning, than platinum on graphite powder.

4. Concluding outlook and future trends

The use of carbon materials as catalyst supports for precious metals rapidly increased in the last years, due to the continuous advancing development of fuel cells. The main requirements of suitable supports for fuel cell catalysts are: high surface area, good electrical conductivity, suitable porosity to allow good reactant flux, and high stability in fuel cell environment. Carbon blacks are commonly used as low-temperature fuel cell catalysts. They are usually submitted to chemical activation to increase anchoring centres for metal catalysts (to increase metal loading and dispersion). The high availability and low cost make carbon blacks the most used support for fuel cell catalysts. The disadvantage of these carbons is the presence of a high amount of micropore, which can hinder the reactant flow. Moreover, these materials present low stability at temperatures higher than 100 °C.

The replacement of carbon blacks by carbon microspheres lead to significant changes in the catalytic layer structure of the fuel cell. Indeed, carbon microspheres have monolithic porous structure whereas carbon blacks are aggregates. The arrangement of the primary carbon nanoparticles which they are both made of, differ greatly. The primary carbon nanoparticles of a carbon black are fused together in clusters of a few tens of particles covalently linked and called aggregates. Such aggregates are usually agglomerated through Van der Waals stabilizing interactions. In the case of carbon microspheres, the primary carbon nanoparticles are tridimensionally linked through covalent bonds to form a macroscopic monolithic structure with high porosity and good electronic conductivity. This particular structure of the carbon microspheres prevents the formation of small or even closed pores (inside aggregates) in the catalytic layer of the fuel cell.

The high surface area and high amount of mesopores of ordered mesoporous carbons and carbon gels allow high metal dispersion and good reactant flux. So, catalysts supported on these carbons showed higher catalytic activity than the same catalysts supported on carbon black. Their thermal stability was almost the same to that of carbon blacks. It has to be remarked that the synthesis methods of ordered mesoporous carbons and carbon cryogels are simple and not too expensive.

Among the new carbon materials, carbon nanotubes are the most investigated as catalyst support for low-temperature fuel cells. The high crystallinity of CNTs make these materials highly conductive, the high surface area and high amount of mesopores result in a high metal dispersion and a good reactant flux in tubular structure. Moreover, CNTs have a positive effect on Pt structure, resulting in a higher catalytic activity and a higher stability than carbon blacks. A problem for the commercialization of carbon nanotubes is their higher cost compared to that of carbon blacks.

Few works have been carried out on carbon nanohorns, carbon nanocoils and carbon fibers as fuel cell catalyst support, but tests in fuel cells of these materials showed promising results. Moreover, conversely to the other types of carbons, an advantage of carbon fibers consists in the following: due to their peculiar structure, ACFs and CNFs can be used as catalytic supports without any pre-treatment.

Regarding boron-doped diamonds, they present high thermal stability, but the anchoring of metal atoms on BDD surface in a

Table 2
Specific surface area, porosity and electronic conductivity of the different carbon materials and properties of supported catalysts.

Carbon material	Specific surface area ($m^2\ g^{-1}$)	Porosity	Electronic conductivity ($S\ cm^{-1}$)	Supported catalyst properties	Refs.
Vulcan XC-72R	254	Microporous	4.0	Good metal dispersion low gas flow	[19,25,219]
OMC	400–1800	Mesoporous	0.3×10^{-2}–1.4	High metal dispersion High gas flow Low metal accessibility	[81,82,87,89–91]
Carbon gels	400–900	Mesoporous	>1	High metal dispersion High gas flow High metal accessibility	[102,107–109,117,119,220]
CNT	400–900 (SWCNT) 200–400 (MWCNT)	Microporous (SWCNT) Mesoporous (MWCNT)	$10–10^4$ depending on nanotube alignment 0.3, 3 (functionalized MWCNTs)	Good metal dispersion high gas flow Low metal accessibility high metal stability	[51,138,150,151,154,173,179]
CNH, CNC	150	Micro/mesoporous	3–200	High metal dispersion high gas flow	[184–187,221]
ACF	>1000	Microporous	13	Good metal dispersion low gas flow High metal stability	[163,165,190,192,222]
CNF	10–300	Mesoporous	10^2–10^4	High metal dispersion High gas flow High metal stability	[60,198,203,138,142,151,223,224]
BDD	2	–	1.5	Low metal dispersion Low metal stability High metal stability on BDD/Nafion	[207]

stable way has to be improved. The use of Nafion as the binder seems to enhance the stability of metal supported catalysts.

The main characteristics of carbon materials and carbon-supported catalysts are reported in Table 2.

Generally, suitable carbon supports must possess high mesoporosity in the pore-size range of 20–40 nm for a high accessible surface area. Indeed, the Nafion binder solution, which is generally used in electrode preparation, is constituted by ionomers that do not enter or may occlude pores narrower than 20 nm, so that catalyst particles chemically deposited in such pores are not in contact with the proton conductor and/or the fuel. For this reason, the presence of mesopores with pore size <20 nm supports the gas flow, but decrease the active surface area of the catalyst. As a consequence the electrochemical activity of these mesoporous carbons could be lower than that of microporous carbons. On the basis of their high versatility in pore size and pore distribution tailoring, among the mesoporous carbons, carbon gels seem more promising than OMCs.

Regarding the CNT, as previously reported, they normally possess outer diameter of 10–50 nm, inside diameter of 3–15 nm (pore size), and a tube length of 10–50 μm. During synthesis of the catalyst using this support, Pt particles (2–5 nm size) present on the pore mouths of CNTs will take part in the chemical reaction. However, there is a great possibility for the existence of Pt particles inside the nanotube, depending on Pt particle size. These particles will take little part in the chemical reaction. The number of the Pt particles inside the tube will be more when the tube length of CNT increases. So, a decrease of the Pt active area and the electrochemical activity of the catalyst have to be expected.

By comparing CNTs and MCs, taking into account of the cost of the materials, the complexity of the synthesis methods, and the versatility in pore size and pore distribution tailoring, the mesoporous carbons seem to have more changes to substitute carbon blacks as fuel cell catalyst substrate. On the other hand, CNTs, for their high electronic conductivity, due to their unique structure, and their high stability during long-term tests in acidic media, ascribed to the strong metal-carbon interactions, seem to be more suitable than MCs for use as a support for fuel cell catalysts. The stability in fuel cell conditions of MC supported metals is similar to that of carbon black supported catalysts, but can be increased by graphitization of the mesoporous carbons.

In the perspective to the replacement carbon blacks with MCs or CNTs as catalyst supports, further tests in fuel cells have to be performed to evaluate the electrochemical activity and the long-term stability of the catalysts supported on these new promising materials.

References

[1] P. Costamagna, S. Srinivasan, J. Power Sources 102 (2001) 242.
[2] X. Ren, P. Zelenay, S. Thomas, J. Davey, S. Gottesfeld, J. Power Sources 86 (2000) 111.
[3] K. Kinoshita, J. Electrochem. Soc. 137 (1990) 845.
[4] M. Watanabe, H. Sei, P. Stonehart, J. Electroanal. Chem. 261 (1989) 375.
[5] K. Yahikozawa, Y. Fujii, Y. Matsuda, K. Nishimura, Y. Takasu, Electrochim. Acta 36 (1991) 973.
[6] A. Kabbabi, F. Gloaguen, F. Andolfatto, R. Durand, J. Electroanal. Chem. 373 (1994) 251.
[7] E. Antolini, J. Mater. Sci. 38 (2003) 2995.
[8] E. Antolini, Mater. Chem. Phys. 78 (2003) 563.
[9] R.L. Augustine, Heterogeneous Catalysis for the Synthetic Chemists, Marcel Dekker, New York, 1996.
[10] K.-W. Park, K.-S. Ahn, Y.-C. Nah, J.-H. Choi, Y.-E. Sung, J. Phys. Chem. B 107 (2003) 4352.
[11] E.J. McLeod, V.I. Birss, Electrochim. Acta 51 (2005) 684.
[12] Z. Chen, X. Qiu, B. Lu, S. Zhang, W. Zhu, L. Chen, Electrochem. Commun. 7 (2005) 593.
[13] H.M. Villullas, F.I. Mattos-Costa, L.O.S. Bulhoes, J. Phys. Chem. B 108 (2004) 12898.
[14] D.A. Stevens, J.R. Dahn, Carbon 43 (2005) 179.
[15] D.A. Stevens, M.T. Hicks, G.M. Haugen, J.R. Dahn, J. Electrochem. Soc. 152 (2005) A2309.
[16] E. Auer, A. Freund, J. Pietsch, T. Tacke, Appl. Catal. A 173 (1998) 259.
[17] F. Rodriguez-Reinoso, Carbon 36 (1998) 159.
[18] O. Wohler, F. von Sturm, E. Wege, H. von Kienle, M. Voll, P. Kleinschmit, in: W. Gerhartz (Ed.), Ullmann's Encyclopaedia of Industrial Chemistry, vol. A5, VCH, Weinheim, 1986, p. 95.
[19] M. Uchida, Y. Aoyama, M. Tanabe, N. Yanagihara, N. Eda, A. Ohta, J. Electrochem. Soc. 142 (1995) 2572.
[20] E. Antolini, R.R. Passos, E.A. Ticianelli, J. Power Sources 109 (2002) 477.
[21] P. Gallezot, S. Chaumet, A. Perrard, P. Isnard, J. Catal. 168 (1997) 104.
[22] D. Richard, P. Gallezot, D. Neibecker, I. Tkatchenko, Catal. Today 6 (1989) 171.
[23] M.A. Fraga, E. Jordao, M.J. Mendes, M.M.A. Freita, J.L. Faria, J.L. Figueredo, J. Catal. 209 (2002) 355.
[24] M. Watanabe, S. Saegusa, P. Stonehart, Chem. Lett. 9 (1988) 1487.
[25] J. McBreen, H. Olender, S. Srinivasan, K. Kordesch, J. Appl. Electrochem. 11 (1981) 787.
[26] V. Rao, P.A. Simonov, E.R. Savinova, G.V. Plaksin, S.V. Cherepanova, G.N. Kryukova, U. Stimming, J. Power Sources 145 (2005) 178.
[27] A. Gamez, D. Richard, P. Gallezot, in Resume des Journees d'Etude Piles a Combustible, Paris, France, 1999, p. 401.
[28] E. Antolini, F. Cardellini, E. Giacometti, G. Squadrito, J. Mater. Sci. 37 (2002) 133.
[29] Y. Takasu, T. Kawaguchi, W. Sugimoto, Y. Murakami, Electrochim. Acta 48 (2003) 3861.
[30] H. Gharibi, R.A. Mirzaie, E. Shams, M. Zhiani, M. Khairmand, J. Power Sources 139 (2005) 61.
[31] F.J. Derbyshire, V.H.J. de Beer, G.M.K. Abotsi, A.W. Scaroni, J.M. Solar, D.J. Skrovanek, Appl. Catal. 27 (1986) 117.
[32] D.S. Cameron, S.J. Cooper, I.L. Dodgson, B. Harrison, J.W. Jenkins, Catal. Today 7 (1990) 113.
[33] G.C. Torres, E.I. Jablonski, G.T. Baronetti, A.A. Castro, S.R. de Miguel, O.A. Scelza, M.D. Blanco, M.A. Pena-Jimenez, J.L.G. Fierro, Appl. Catal. A 161 (1997) 213.
[34] C. Prado-Burguete, A. Linares-Solano, F. Rodriguez-Reinoso, C.S.M. Lecea, J. Catal. 115 (1989) 98.
[35] D.J. Suh, T.J. Park, S.K. Ihm, Carbon 31 (1993) 427.
[36] S.R. Miguel, O.A. Scelza, M.C. Roman-Martinez, C.S.M. Lecea, D. Cazorla-Amoros, A. Linares-Solano, Appl. Catal. A 170 (1998) 93.
[37] A. Sepulveda-Escribano, F. Coloma, F. Rodriguez-Reinoso, Appl. Catal. A 173 (1998) 247.
[38] A. Guerrero-Ruiz, P. Badenes, I. Rodriguez-Ramos, Appl. Catal. A 173 (1998) 313.
[39] P. Ehrburger, O.P. Majahan, P.L. Walker, J. Catal. 43 (1976) 61.
[40] C. Coloma, A. Sepulveda-Escribano, J.L. Fierro, F. Rodriguez-Reinoso, Langmuir 10 (1994) 750.
[41] M.C. Roman-Martinez, D. Cazorla-Amoros, A. Linares-Solano, C.S.M. Lecea, H. Yamashita, M. Anpo, Carbon 33 (1995) 3.
[42] C.K. Poh, S.H. Lim, H. Pan, J. Lin, J.Y. Lee, J. Power Sources 176 (2008) 70.
[43] Z.B. Wang, G.P. Yin, P.F. Shi, Carbon 44 (2006) 133.
[44] H. Shioyama, K. Honjo, M. Kiuchi, Y. Yamada, A. Ueda, N. Kurijama, T. Kobayashi, J. Power Sources 161 (2006) 836.
[45] S. Kim, S.J. Park, J. Power Sources 159 (2006) 42.
[46] S. Kim, S.J. Park, Electrochim. Acta 52 (2007) 3013.
[47] J.L. Gómez de la Fuente, S. Rojas, M.V. Martínez-Huerta, P. Terreros, M.A. Peña, J.L.G. Fierro, Carbon 44 (2006) 1919.
[48] H.K. Kim, W. Li, D. Yoo, Electrochim. Acta 52 (2007) 2620.
[49] G. Selvarani, A.K. Sahu, N.A. Choudhuri, P. Sridhar, S. Pitchumani, A.K. Shukla, Electrochim. Acta 52 (2007) 4871.
[50] T. Maiyalagan, B. Viswanathan, Mater. Chem. Phys. 93 (2005) 291.
[51] T. Maiyalagan, B. Viswanathan, U.V. Varadaraju, Electrochem. Commun. 7 (2005) 905.
[52] B. Choi, H. Yoon, I.S. Park, J. Jang, Y.E. Sung, Carbon 45 (2007) 2496.
[53] A.L.N. Pinheiro, A. Oliveira-Neto, E.C. de Souza, J. Perez, V.A. Paganin, E.A. Ticianelli, E.R. Gonzalez, J. New Mater. Electrochem. Syst. 6 (2003) 1.
[54] X. Yu, S. Ye, J. Power Sources 172 (2007) 133.
[55] G.A. Gruver, J. Electrochem. Soc. 125 (1978) 1719.
[56] J. Wang, G. Yin, Y. Shao, S. Zhang, Z. Wang, Y. Gao, J. Power Sources 171 (2007) 331.
[57] P. Stonehart, Carbon 22 (1984) 423.
[58] K.W. Park, Y.E. Sung, S. Han, Y. Yun, T. Hyeon, J. Phys. Chem. B 108 (2004) 939.
[59] W.H. Zhang, J.L. Shi, L.Z. Wang, D.S. Yan, Chem. Mater. 12 (2000) 1408.
[60] C.A. Bessel, K. Laubernds, N.M. Rodriguez, R.T.K. Baker, J. Phys. Chem. B 105 (2001) 1115.
[61] E.S. Steigerwalt, G.A. Deluga, C.M. Lukehart, J. Phys. Chem. B 106 (2002) 760.
[62] W.Z. Li, C.H. Liang, J.S. Qiu, W.J. Zhou, H.M. Han, Z.B. Wie, G.Q. Sun, Q. Xin, Carbon 40 (2002) 791.
[63] Y.C. Liu, X.P. Qiu, Y.Q. Huang, W.T. Zhu, Carbon 40 (2002) 2375.
[64] K.I. Han, J.S. Lee, S.O. Park, S.W. Lee, Y.M. Park, H. Kim, Electrochim. Acta 50 (2004) 791.
[65] R.V. Hull, L. Li, Y. Xing, C.C. Chusuei, Chem. Mater. 18 (2006) 1780.
[66] R. Ryoo, S.H. Joo, M. Kruk, M. Jaroniec, Adv. Mater. 13 (2001) 677.
[67] S.I. Kim, T. Yamamoto, A. Endo, T. Ohmori, M. Nakaiwa, J. Ind. Eng. Chem. 12 (2006) 769.
[68] F. Su, X. Li, L. Lv, X.S. Zhao, Carbon 44 (2006) 801.
[69] X. Huang, Y. Li, H. Im, O. Yarimaga, J. Kim, D. Jang, S. Cho, W. Cai, Y. Choi, Nanotechnology 17 (2006) 2988.
[70] M. Han, W. Zhang, C. Gao, Y. Liang, Z. Xu, J. Zhu, J. He, Carbon 44 (2006) 211.

[71] J.H. Bang, K. Han, S.E. Skrabalak, H. Kim, K.S. Suslick, J. Phys. Chem. C 111 (2007) 10959.
[72] S.E. Skrabalak, K.S. Suslick, J. Am. Chem. Soc. 128 (2006) 12642.
[73] C. Xu, Y. Liu, D. Yuan, Int. J. Electrochem. Sci. 2 (2007) 674.
[74] C. Xu, L. Cheng, P. Shen, Y. Liu, Electrochem. Commun. 9 (2007) 97.
[75] R.Z. Yang, X.P. Qiu, H.R. Zhang, J.Q. Li, W.T. Zhu, Z.X. Wang, X.J. Huang, L.Q. Chen, Carbon 43 (2005) 11.
[76] Z. Wen, Q. Wang, Q. Zhang, J. Li, Electrochem. Commun. 9 (2007) 1867.
[77] B. Fang, J.H. Kim, C. Lee, J.S. Yu, J. Phys. Chem. C 112 (2008) 639.
[78] S.H. Joo, S.J. Choi, I. Oh, J. Kwak, Z. Liu, O. Terasaki, R. Ryoo, Nature 412 (2001) 169.
[79] F.B. Su, J.H. Zeng, X.Y. Bao, Y.S. Yu, J.Y. Lee, X.S. Zhao, Chem. Mater. 17 (2005) 3960.
[80] A. Stein, Adv. Mater. 15 (2003) 763.
[81] H. Chang, S.H. Joo, C. Pak, J. Mater. Chem. 17 (2007) 3078.
[82] S. Jun, S.H. Joo, R. Ryoo, M. Kruk, M. Jaroniec, Z. Liu, T. Ohsuna, O. Terasaki, J. Am. Chem. Soc. 122 (2000) 10712.
[83] D. Zhao, Q. Huo, J. Feng, B.F. Chmelka, G.D. Stucky, J. Am. Chem. Soc. 120 (1998) 6024.
[84] H.J. Shin, R. Ryoo, M. Kruk, M. Jaroniec, Chem. Commun. (2001) 349.
[85] R. Ryoo, S.H. Joo, S. Jun, J. Phys. Chem. B 103 (1999) 7743.
[86] J.M. Kim, G.D. Stucky, Chem. Commun. (2000) 1159.
[87] L. Calvillo, M.J. Lazaro, E. Garcýa-Bordeje, R. Moliner, P.L. Cabot, I. Esparbe, E. Pastor, J.J. Quintana, J. Power Sources 169 (2007) 59.
[88] J.S. Choi, W.S. Chung, H.Y. Ha, T.H. Lim, I.H. Oh, S.A. Hong, H.I. Lee, J. Power Sources 156 (2006) 466.
[89] A.B. Fuertes, S. Alvarez, Carbon 42 (2004) 3049.
[90] L. Wang, S. Lin, K. Lin, C. Yin, D. Liang, Y. Di, P. Fan, D. Jiang, F.S. Xiao, Microporous Mesoporous Mater. 85 (2005) 136.
[91] V. Raghuveer, A. Manthiram, Electrochem. Sol. State Lett. 7 (2004) A336.
[92] V. Raghuveer, A. Manthiram, J. Electrochem. Soc. 152 (2005) A1504.
[93] C. Liang, S. Daí, J. Am. Chem. Soc. 128 (2006) 5319.
[94] S. Tanaka, N. Nishiyama, Y. Egashira, K. Ueyama, Chem. Commun. (2005) 2125.
[95] F. Zhang, Y. Meng, D. Gu, Y. Yan, C. Yu, B. Tu, D. Zhao, J. Am. Chem. Soc. 127 (2005) 13508.
[96] R. Ryoo, S.H. Joo, S. Jun, T. Tsubakiyama, O. Terasaki, Stud. Surf. Sci. Catal. 135 (2001) 1121.
[97] J. Ding, K.Y. Chan, J.W. Ren, F.S. Xiao, Electrochim. Acta 50 (2005) 3131.
[98] S.H. Joo, C. Pak, D.J. You, S.A. Lee, H.I. Lee, J.M. Kim, H. Chang, D. Seung, Electrochim. Acta 52 (2006) 1618.
[99] H. Yamada, T. Hirai, I. Moriguchi, T. Kudo, J. Power Sources 164 (2007) 538.
[100] S. Vengatesan, H.J. Kim, S.K. Kim, I.H. Oh, S.Y. Lee, Electrochim. Acta 54 (2008) 856.
[101] A. Hayashi, H. Notsu, K. Kimijima, J. Miyamotoa, I. Yagi, Electrochim. Acta 53 (2008) 6117.
[102] C. Moreno-Castilla, F.J. Maldonado-Hódar, Carbon 43 (2005) 455.
[103] R.W. Pekala, J. Mater. Sci. 24 (1989) 3221.
[104] C.J. Brinker, G.W. Scherer, Sol Gel Science, Academic Press, San Diego, CA, 1990
[105] H. Tamon, H. Ishizaka, T. Yamamoto, T. Suzuki, Carbon 37 (1999) 2049.
[106] E.J. Zanto, S.A. Al-Muhtaseb, J.A. Ritter, Ind. Eng. Chem. Res. 41 (2002) 3151.
[107] J. Marie, S. Berthon-Fabry, M. Chatenet, E. Chainet, R. Pirard, N. Cornet, P. Achard, J. Appl. Electrochem. 37 (2007) 147.
[108] N. Job, F. Panariello, J. Marien, M. Crine, J.-P. Pirard, A. Leonard, J. Non-Cryst. Solids 352 (2006) 24.
[109] T. Yamamoto, T. Nishimura, T. Suzuki, H. Tamon, J. Non-Cryst. Solids 288 (2001) 46.
[110] B. Babic, B. Kaluderovic, L. Vracar, N. Krstajic, Carbon 42 (2004) 2617.
[111] T. Yamamoto, T. Sugimoto, T. Suzuki, S.R. Mukai, H. Tamon, Carbon 40 (2002) 1345.
[112] H. Hasegawa, S.R. Mukai, Y. Shirato, H. Tamon, Carbon 42 (2004) 2573.
[113] N. Job, A. Thery, R. Pirard, J. Marien, L. Kocon, J.N. Rouzaud, F. Beguin, J.P. Pirard, Carbon 43 (2005) 2481.
[114] T. Yamamoto, A. Endo, T. Ohmori, M. Nakaiwa, Carbon 43 (2005) 1231.
[115] S.I. Kim, T. Yamamoto, A. Endo, T. Ohmori, M. Nakaiwa, J. Ind. Eng. Chem. 12 (2006) 484.
[116] P. Kim, H. Kim, J.B. Joo, W. Kim, I.K. Song, J. Yi, J. Power Sources 145 (2005) 139.
[117] Z. Zhou, W. Zhou, S. Wang, G. Wang, L. Jiang, H. Li, G. Sun, Q. Xin, Catal. Today 93 (2004) 523.
[118] B.M. Babić, Lj.M. Vračar, V. Radmilović, N.V. Krstajić, Electrochim. Acta 51 (2006) 3820.
[119] C. Arbizzani, S. Beninati, E. Manferrari, F. Soavi, M. Mastragostino, J. Power Sources 161 (2006) 826.
[120] C. Arbizzani, S. Beninati, E. Manferrari, F. Soavi, M. Mastragostino, J. Power Sources 172 (2007) 578.
[121] E. Guilminot, F. Fischer, M. Chatenet, A. Rigacci, S. Berthon-Fabry, P. Achard, E. Chainet, J. Power Sources 166 (2007) 104.
[122] H.D. Du, B.H. Li, F.Y. Kang, R.W. Fu, Y.Q. Zeng, Carbon 45 (2007) 429.
[123] J. Marie, S. Berthon-Fabry, P. Achard, M. Chatenet, A. Pradourat, E. Chainet, J. Non-Cryst. Solids 350 (2004) 88.
[124] P.V. Shanahan, L. Xu, C. Liang, M. Waje, S. Dai, Y.S. Yan, J. Power Sources 185 (2008) 423.
[125] D.J. Guo, H.L. Li, J. Power Sources 160 (2006) 44.
[126] G. Che, B.B. Lakshmi, E.R. Fisher, C.R. Martin, Nature 393 (1998) 346.
[127] G. Che, B.B. Lakshmi, C.R. Martin, E.R. Fisher, Langmuir 15 (1999) 750.
[128] B. Rajesh, V. Karthik, S. Karthikeyan, K.R. Thampi, J.M. Bonard, B. Viswanathan, Fuel 81 (2002) 2177.
[129] Z.L. Liu, X.H. Lin, J.Y. Lee, W.D. Zhang, M. Han, L.M. Gan, Langmuir 18 (2002) 4054.
[130] S.L. Knupp, W. Li, O. Paschos, T.M. Murray, J. Snyder, P. Haldar, Carbon 46 (2008) 1276.
[131] T. Matsumoto, T. Komatsu, H. Nakano, K. Arai, Y. Nagashima, E. Yoo, T. Yamazaki, M. Kijima, H. Shimizu, Y. Takasawa, J. Nakamura, Catal. Today 90 (2004) 277.
[132] C. Kim, Y.J. Kim, Y.A. Kim, T. Yanagisawa, K.C. Park, M. Endo, M.S. Dresselhaus, J. Appl. Phys. 96 (2004) 5903.
[133] Y. Xing, J. Phys. Chem. B 108 (2004) 19255.
[134] C. Wang, M. Waje, X. Wang, J.M. Tang, C.R. Haddon, Y. Yan, Nano Lett. 4 (2004) 345.
[135] M. Carmo, V.A. Paganin, J.M. Rosolen, E.R. Gonzalez, J. Power Sources 142 (2005) 169.
[136] P.M. Ajayan, in: H.S. Nalwa (Ed.), Nanostructured Materials and Nanotechnology, Concise edn., Academic Press, San Diego, 2002 , p. 332 (Chapter 8).
[137] J. Fan, C. Yu, F. Gao, J. Lei, B. Tian, L. Wang, Q. Luo, B. Tu, W. Zhou, D. Zhao, Angew. Chem. Int. Ed. 42 (2003) 3146.
[138] P. Serp, M. Corrias, P. Kalck, Appl. Catal. A 253 (2003) 337.
[139] M. Eswaramoorthy, R. Sen, C.N.R. Rao, Chem. Phys. Lett. 304 (1999) 207.
[140] R. Saito, M. Fujita, G. Dresselhaus, M. Dresselhaus, Appl. Phys. Lett. 60 (1992) 2204.
[141] A.Y. Kasumov, H. Bouchiat, B. Reulet, O. Stephan, I.I. Khodos, Y.B. Gorbatov, C. Colliex, Europhys. Lett. 43 (1998) 89.
[142] T.W. Ebbesen, P.M. Ajayan, Nature 358 (1992) 220.
[143] A. Thess, R. Lee, P. Nikolaev, H. Dai, P. Petit, J. Robert, C. Xu, Y.H. Lee, S.G. Kim, A.G. Rinzler, D.T. Colbert, G.E. Scuseria, D. Tománek, J.E. Fischer, R.E. Smalley, Science 273 (1996) 483.
[144] H. Dai, in: M.S. Dresselhouse, G. Dresselhouse, P. Avouris (Eds.), Carbon Nanotubes: Synthesis, Structure, Properties and Application, Springer, New York, 2001, p. 29.
[145] Z.F. Ren, Z.P. Huang, J.W. Xu, J.H. Wang, P. Bush, M.P. Siegal, P.N. Provencio, Science 282 (1998) 1105.
[146] M. Chhowalla, K.B.K. Teo, C. Ducati, N.L. Rupesinghe, G.A.J. Amaratunga, A.C. Ferrari, D. Roy, J. Robertson, W.I. Milne, J. Appl. Phys. 90 (2001) 5308.
[147] S. Hofmann, C. Ducati, B. Kleinsorge, J. Robertson, Appl. Phys. Lett. 83 (2003) 135.
[148] W.Z. Li, C.H. Liang, W.J. Zhou, J.S. Qiu, Z.H. Zhou, G.Q. Sun, J. Phys. Chem. B 107 (2003) 6292.
[149] S. Hofmann, C. Ducati, B. Kleinsorge, J. Robertson, Appl. Phys. Lett. 83 (2003) 4661.
[150] G.G. Wildgoose, C.E. Banks, R.G. Compton, Small 2 (2006) 182.
[151] K. Lee, J. Zhang, H. Wang, D.P. Wilkinson, J. Appl. Electrochem. 36 (2006) 507.
[152] W. Li, C. Liang, W. Zhou, J. Qiu, H. Li, G. Sun, Q. Xin, Carbon 42 (2004) 436.
[153] T. Matsumoto, T. Komatsu, K. Arai, T. Yamazaki, M. Kijima, H. Shimizu, Chem. Commun. (2004) 840.
[154] J. Prabhuram, T.S. Zhao, Z.K. Tang, R. Chen, Z.X. Liang, J. Phys. Chem. B 110 (2006) 5245.
[155] B. Zhang, L.J. Chen, K.Y. Ge, Y.C. Guo, B.X. Peng, Chin. Chem. Lett. 16 (2005) 1531.
[156] Z.D. Wei, C. Yan, Y. Tan, L. Li, C.X. Sun, Z.G. Shao, P.K. Shen, H.W. Dong, J. Phys. Chem. C 112 (2008) 2671.
[157] M.S. Saha, R. Li, X. Sun, J. Power Sources 177 (2008) 314.
[158] S.D. Oh, B.K. So, S.H. Choi, A. Gopalan, K.P. Lee, K.R. Yoon, Z.S. Choi, Mater. Lett. 59 (2005) 1121.
[159] J.L. Hudson, M.J. Casavant, J.M. Tour, J. Am. Chem. Soc. 126 (2004) 11158.
[160] J.J. Stephenson, J.L. Hudson, S. Azad, J.M. Tour, Chem. Mater. 18 (2006) 374.
[161] S. Yang, X. Zhang, H. Mi, X. Ye, J. Power Sources 175 (2008) 26.
[162] C.Y. Du, T.S. Zhao, Z.X. Liang, J. Power Sources 176 (2008) 9.
[163] E. Yoo, T. Okada, T. Kizuka, J. Nakamura, J. Power Sources 180 (2008) 221.
[164] K. Ke, K. Waki, J. Electrochem. Soc. 154 (2007) A207.
[165] W. Li, C. Liang, J. Qiu, W. Zhou, H. Han, Z. Wei, G. Sun, Q. Xin, Carbon 40 (2002) 791.
[166] X. Wang, M. Waje, Y. Yan, Electrochem. Solid State Lett. 8 (2005) A42.
[167] J.J. Wang, G.P. Yin, J. Zhang, Z.B. Wang, Y.Z. Gao, Electrochim. Acta 52 (2007) 7042.
[168] D.J. Guo, L. Zhao, X.P. Qiu, L.Q. Chen, W.T. Zhu, J. Power Sources 177 (2008) 334.
[169] H.T. Zheng, Y. Li, S. Chen, P.K. Shen, J. Power Sources 163 (2006) 371.
[170] S. Liao, K. Holmes, H. Tsaprailis, V.I. Birss, J. Am. Chem. Soc. 128 (2006) 3504.
[171] A. Kongkanand, S. Kuwubata, G. Girishkumar, P. Kamat, Langmuir 22 (2006) 2392.
[172] O. Paschos, S.L. Knupp, P. Choi, J. Snyder, S.J. Buelte, N. Merchant, Z. Qi, P. Haldar, Electrochem Solid State Lett. 10 (2007) B147.
[173] E. Bekyarova, M.E. Itkis, N. Cabrera, B. Zhao, A. Yu, J. Gao, R.C. Haddon, J. Am. Chem. Soc. 127 (2005) 5995.
[174] B. Rajesh, K. Ravindranathan Thampi, J.-M. Bonard, N. Xanthopoulos, H.J. Mathieu, B. Viswanathan, J. Phys. Chem. B 107 (2003 2701).
[175] J.W. Long, R.M. Stroud, K.E. Swider-Lyons, D.R. Rolison, J. Phys. Chem. B 104 (2000) 9772.
[176] T. Maiyalagan, Appl. Catal. B 80 (2008) 286.
[177] H.Y. Du, C.H. Wang, H.C. Hsu, S.T. Chang, U.S. Chen, S.C. Yen, L.C. Chen, H.C. Shih, K.H. Chen, Diamond Related Mater. 17 (2008) 535.
[178] G. Wu, B.Q. Xu, J. Power Sources 174 (2007) 148.
[179] X. Wang, W. Li, Z. Chen, M. Waje, Y. Yan, J. Power Sources 158 (2006) 154.
[180] D. Kasuya, M. Yudasaka, K. Takahashi, F. Kokai, S. Iijima, J. Phys. Chem. B 106 (2002) 4947.
[181] M. Yudasaka, J.A. Nisha, D. Kauya, F. Kokai, K. Takahashi, K. Hirahara, S. Iijima, American Physical Society Annual March Meeting, March 12–16, Seattle, Washington, USA, 2001.

[182] Y.C. Choi, E. Lee, H. Vedala, W.B. Choi, Second LACCEI International Latin American and Caribbean Conference for Engineering and Technology (LACCEI'2004), 2–4 June 2004, Miami, Florida, USA, 2004.
[183] X. Chen, S. Zhang, D.A. Dikin, W. Ding, E.S. Ruoff, L. Pan, Y. Nakayama, Nano Lett. 3 (2003) 1299.
[184] N. Sano, S. Ukita, Mater. Chem. Phys. 99 (2006) 447.
[185] T. Yoshitake, Y. Shimakawa, S. Kuroshima, H. Kimura, T. Ichihashi, Y. Kubo, D. Kasuya, K. Takahashi, F. Kokai, M. Yudasaka, S. Iijima, Phys. B: Cond. Matter 323 (2002) 124.
[186] T.H. Hyeon, S.J. Han, Y.E. Sung, K.W. Park, Y.W. Kim, Angew. Chem. Int. Ed. 42 (2003) 4352.
[187] M. Sevilla, G. Lota, A.B. Fuertes, J. Power Sources 171 (2007) 546.
[188] F. Parmentier, J.P. Joly, A. Perrard, U.S. Patent 6,383,972 (2000).
[189] D.A. Bulushev, I. Yuranov, E.I. Suvorova, P.A. Buffat, L. Kiwi-Minsker, J. Catal. 224 (2004) 8.
[190] H.X. Huang, S.X. Chen, C. Yuan, J. Power Sources 175 (2008) 166.
[191] S. Chen, R. Xu, H. Huang, F. Yi, X. Zhou, H. Zeng, J. Mater. Sci. 42 (2007) 9572.
[192] S.R. de Miguel, J.I. Villella, E.L. Jablonski, O.A. Scelza, C.S.M. de Lecea, A. Linares-Solano, Appl. Catal. A 232 (2002) 237.
[193] N.M. Rodriguez, A. Chambers, R.T.K. Baker, Langmuir 11 (1995) 3862.
[194] C. Park, R.T.K. Baker, J. Phys. Chem. B 102 (1998) 5168.
[195] C. Park, R.T.K. Baker, J. Phys. Chem. B 103 (1999) 2453.
[196] E.S. Steigerwalt, G.A. Deluga, D.E. Cliffel, C.M. Lukehart, J. Phys. Chem. B 105 (2001) 8097.
[197] I.S. Park, K.W. Park, J.H. Choi, C.R. Park, Y.E. Sung, Carbon 45 (2007) 28.
[198] W.B. Downs, R.T.K. Baker, J. Mater. Res. 10 (1995) 625.
[199] W.B. Downs, R.T.K. Baker, Carbon 29 (1991) 1173.
[200] B.O. Boskovic, V.B. Golovko, M. Cantoro, B. Kleinsorge, A.T.H. Chuang, C. Ducati, S. Hofmann, J. Robertson, B.F.G. Johnson, Carbon 43 (2005) 2643.
[201] B.O. Boskovic, V. Stolojan, R.U.A. Khan, S. Haq, S.R.P. Silva, Nat. Mater. 1 (2002) 165.
[202] M. Gangeri, G. Centi, A. La Malfa, S. Perathoner, R. Vieira, C. Pham-Huu, M.J. Ledoux, Catal. Today 102/103 (2005) 50.
[203] F. Yuan, H. Ryu, Nanotechnology 15 (2004) S596.
[204] N.M. Rodriguez, M.S. Kim, R.T.K. Baker, J. Phys. Chem. 98 (1994) 13108.
[205] J. Xu, M.C. Granger, Q. Chen, T.E. Lister, J.W. Strojek, G.M. Swain, Anal. Chem. 69 (1997) 591.
[206] Q. Chen, M.C. Granger, T.E. Lister, G.M. Swain, J. Electrochem. Soc. 144 (1997) 3806.
[207] A.E. Fischer, G.M. Swain, J. Electrochem. Soc. 152 (2005) B369.
[208] M. Awada, J.W. Strojek, G.M. Swain, J. Electrochem. Soc. 142 (1995) L42.
[209] J.A. Bennett, Y. Show, S.H. Wang, G.M. Swain, J. Electrochem. Soc. 152 (2005) E184.
[210] K. Honda, M. Yoshimura, T.N. Rao, D.A. Tryk, A. Fujishima, K. Yasui, Y. Sakamoto, K. Nishio, H. Masuda, J. Electroanal. Chem. 514 (2001) 35.
[211] J. Wang, G.M. Swain, T. Tachibana, K. Kobashi, J. New Mater. Electrochem. Syst. 3 (2000) 75.
[212] F. Montilla, E. Morallón, I. Duo, Ch. Comninellis, J.L. Vázquez, Electrochim. Acta 48 (2003) 3891.
[213] G.R. Salazar-Banda, H.B. Suffredini, L.A. Avaca, J. Braz. Chem. Soc. 16 (2005) 50.
[214] H.B. Suffredini, V. Tricoli, N. Vatistas, L.A. Avaca, J. Power Sources 158 (2006) 124.
[215] G.R. Salazar-Banda, H.B. Suffredini, M.L. Calegaro, S.T. Tanimoto, L.A. Avaca, J. Power Sources 162 (2006) 9.
[216] G. Siné, G. Foti, Ch. Comninellis, J. Electroanal. Chem. 595 (2006) 115.
[217] G. Siné, D. Smida, M. Limat, G. Foti, Ch. Comninellis, J. Electrochem. Soc. 154 (2007) B170.
[218] N. Spataru, X. Zhang, T. Spataru, D. Tryk, A. Fujishima, J. Electrochem. Soc. 155 (2008) B264.
[219] D. Pantea, H. Darmstadt, S. Kaliaguine, L. Sümmchen, C. Roy, Carbon 39 (2001) 1147.
[220] A.W.P. Fung, G.A.M. Reynolds, Z.H. Wang, M.S. Dresselhaus, G. Dresselhaus, R.W. Pekala, J. Non-Cryst. Solids 186 (1995) 200.
[221] T. Hayashida, L. Pan, Y. Nakayama, Physica B 332 (2002) 352.
[222] J. Jang, S.K. Ryu, J. Mater. Proc. Technol. 180 (2006) 66.
[223] B.J. Kim, S.J. Park, Nanotechnology 17 (2006) 4395.
[224] C. Pham-Huu, N. Keller, G. Ehret, L.J. Charbonniere, R. Ziessel, M.J. Ledoux, J. Mol. Catal. A 170 (2001) 155.